Doctoral thesis

Development of a drug screening method using single-molecule imaging

Daisuke Watanabe

Graduate School of Frontier Biosciences,
Osaka University

Contents

Abbreviations

EGF: Epidermal growth factor

EGFR: Epidermal growth factor receptor

NSCLC: Non-small cell lung cancer

MSD: Mean squared displacement

TIRFM: Total internal reflection fluorescence microscope

AiSIS: Automated intracellular Single-molecule Imaging System

TKI: Tyrosine kinase inhibitor

HTS: High-throughput screening

Abstract

Single-molecule imaging visualizes individual molecules in living cells, providing a lot of insights in the functions of various proteins. Applications of this method to studies of membrane receptors have shown that the lateral diffusion mobility and cluster formation correlate the protein phosphorylation and the downstream signaling, respectively. These results instigated me to apply a large-scale single-molecule analysis, which can be achieved by an automated system, for evaluation of drug effects on the protein activities. In this study, I tried to perform a drug screening by the automated system (AiSIS) based on the single-molecule tracking of receptor behavior on the cell membrane. I targeted epidermal growth factor receptor (EGFR), which is a receptor tyrosine kinase and one of the target molecules in drug exploration because its overexpression and/or mutations are found in various cancers. The screening was performed on 1,134 FDA-approved drugs containing EGFR tyrosine kinase inhibitors (TKIs) and selected hit compounds with significant changes in the EGFR mobility and clustering. These compounds expectedly contained all the EGFR TKIs, which suppressed the mobility decrease by the ligand-induced phosphorylation. The other compounds caused mobility changes regardless of the phosphorylation, and almost all of them triggered EGFR internalization and declined the cell viability. The results suggest that single-molecule screening can identify drugs acting not only on the EGFR phosphorylation, which can be detected by conventional methods, but also on several events in the signal transduction. This method enables to find novel drugs effective for related receptors with previously undefined mechanism.

Chapter 1

General introduction

1.1 Drug discovery of membrane protein

Membrane proteins are proteins that function on the cell membrane, playing critical roles in energy synthesis, ion or nutrient transport and signal transduction etc. Due to their essential functions in vital biological activities, abnormalities in these proteins can lead to various diseases. Therefore, many drugs target membrane proteins, as approximately 60% of currently drugs to act on these proteins include receptors, ion channels, and transporters [1], [2], [3], [4]. Abnormalities in these receptors including tyrosine kinase receptors and G-protein coupled receptor (GPCR) are known to concern with diseases such as cancer, neurodegenerative disorders and autoimmune diseases. Thus, cell membrane receptors are one of the important targets for drug discovery.

Fig1.1

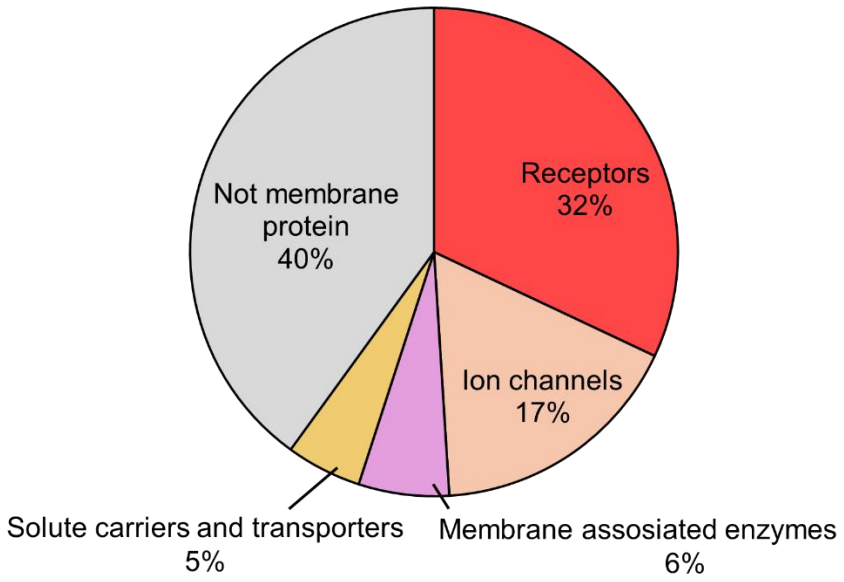

Fig. 1.1 Classes of drug target

Classification and proportions of proteins targeted by marketed drugs are shown. Approximately 60% of these are proteins in the cell membrane.

1.2 Epidermal Growth Factor Receptor for Drug discovery Target

Epidermal growth factor receptor (EGFR) is a type of receptor tyrosine kinase that plays critical roles in cellular growth, survival, and so on. Mutations or overexpression of EGFR can lead to various types of cancer, being a prominent target in drug discovery[5], [6], [7]. Mutations in the kinase domain of EGFR can result in its activation even in the absence of EGF stimulation, and this constitutive activation causes non-small cell lung cancer (NSCLC)[8].

Fig1.2

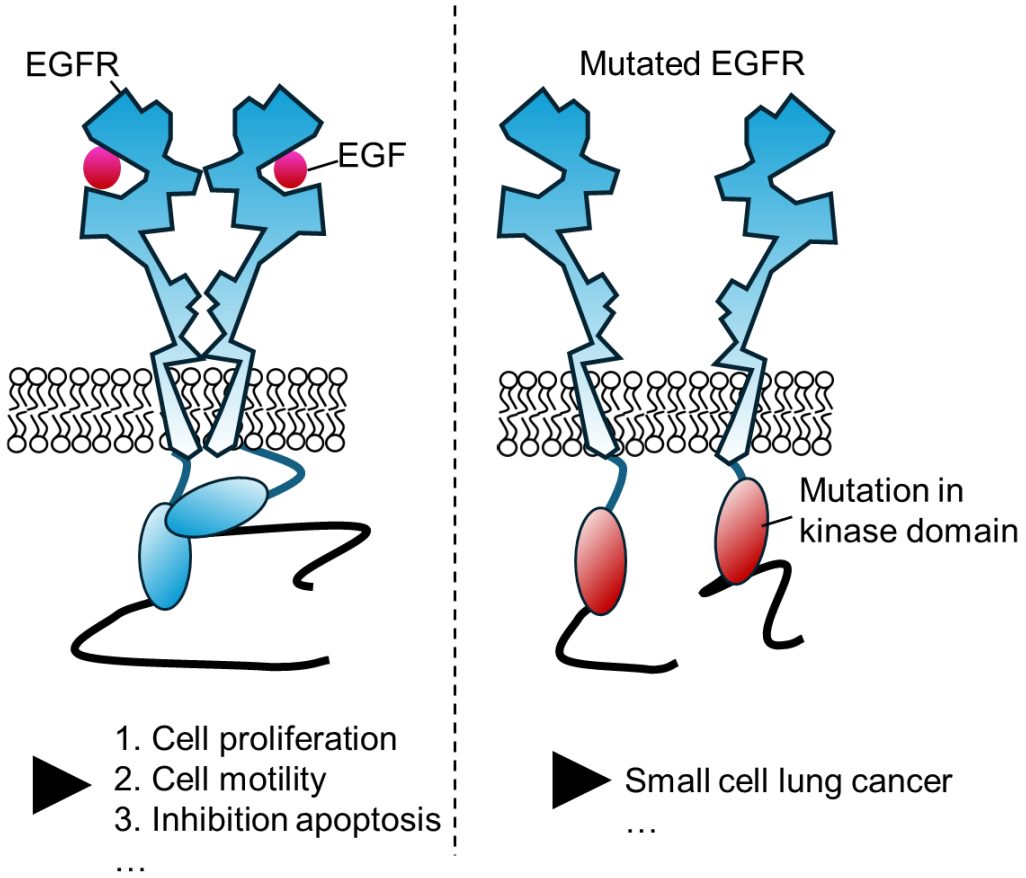

Fig. 1.2 A schematic diagram of EGFR.

The left panel represents normal EGFR. Right panel depicts EGFR with a mutation in the kinase domain. The mutated EGFR is activated even in the absence of EGF.

Clinical data indicate that EGFR mutations are observed in approximately 53% of non-small cell lung cancer (NSCLC) cases. Among these, exon 19 deletions (Del19) account for 44.8%, exon 21 L858R point mutations represent 39.8%, and exon 20 insertion mutations make up 5.8%[9]. These mutations induce structural changes in the ATP-binding site, increasing its affinity for ATP compared to the wild-type receptor[10]. As a result, EGFR undergo constitutive phosphorylation even in the absence of ligand stimulation.

Fig1.3

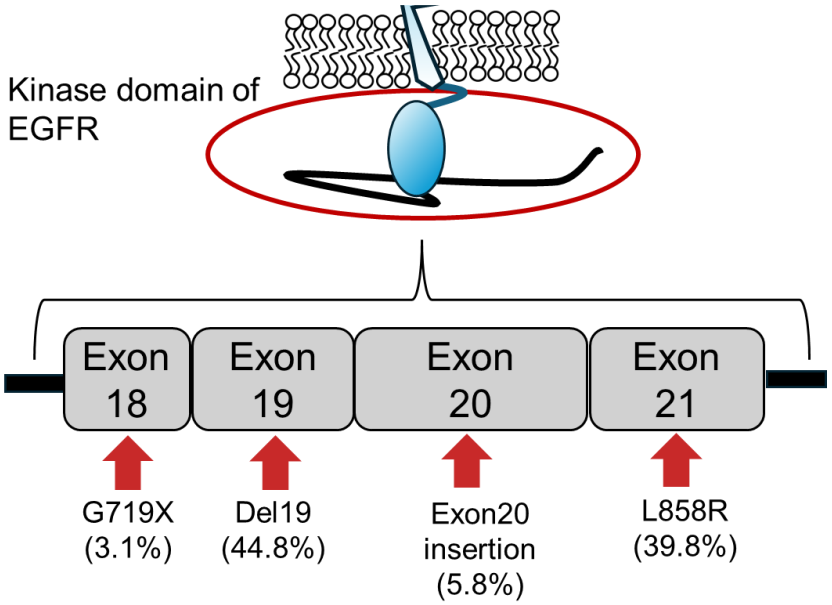

Fig. 1.3 Gene mutation sites of EGFR associated with cancer.

The blue region indicates the kinase domain. G719X represents G719A, G719C, or G719S mutation. Del19 is a deletion mutation involving approximately 5 amino acids in Exon 19. Exon 20 insertion refers to mutations where 1–2 amino acids are inserted. L858R is a mutation in Exon 21 where leucine (L) at position 858 is replaced to arginine (R).

For this background, drugs targeting EGFR mutations has been discovered. Gefitinib, an EGFR tyrosine kinase inhibitor (TKI), was first approved in Japan in 2002, and several TKI has been discovered [9]. While gefitinib is effective against the L858R mutation, resistance has been reported to occur during the treatment. This resistance is caused from double mutations, such as L858R and T790M [11]. In 2016, osimertinib, a drug designed to target such double-mutant EGFRs, was approved. Additionally, EGFR overexpression has also been observed in cancers such as colorectal cancer [12], for which cetuximab, an antibody drug, prevents from EGF binding by competitive inhibition. This inhibition suppresses EGFR-mediated signaling, thereby reducing excessive cell proliferation.

Although the development of EGFR-targeted therapies has progressed, drug resistance in lung cancer appeared during the therapies remains a significant concern. Therefore, the drug discovery for EGFR should be continued in a vicious circle. There are traditional methods for identifying EGFR-targeting such as ELIZA that purify the kinase domain and directly measure its interaction with compounds [13]. These phosphorylation-focused approaches have led to the discovery of the kinase inhibitors. On the other hand, EGFR functions through multiple signaling processes including tyrosine phosphorylation, oligomerization, binding to downstream molecules, and internalization [14]. Therefore, it seems useful for drug discovery to evaluate multiple signaling events as well as to focus on a single step in the processes like a conventional assay. Assays identifying compounds that effect on multiple steps in the processes might have the potential to uncover first-in-class drugs with unique mechanisms of action.

1.2 Single molecule study about EGFR

Single-molecule imaging is a type of super-resolution microscopy that visualizes fluorescently labeled proteins at a single-molecule level typically using total internal reflection fluorescence microscopy (TIRF) for observation of the molecules on the basal cell membrane [15], [16],[17]. This technique enables the measurement of position and fluorescence intensities of single fluorescence spot, providing information of molecular mobility behaviors and oligomerization, respectively.

Studies using this approach have revealed that the ligand(e.g. EGF) binding, decreased the diffusion range of epidermal growth factor receptor (EGFR) on the cell membrane and increases the fluorescence intensity due to oligomer formation[18], [19], [20],[21], [22]. The EGF binding has known to form more dimers and oligomers, undergo phosphorylation, and initiate downstream signaling. During this process, EGFR might move between membrane domains confining the EGFR mobility, such as lipid rafts, with forming clusters that are related to internalization.

Experiments using single molecule imaging with EGFR mutants related to its structure have provided the following insights: mutants lacking the "dimerization arm" responsible for dimer formation showed no change upon EGF stimulation. Additionally, EGFR mutants lacking kinase domain did not exhibit slowed diffusion after EGF stimulation[18]. In experiments removing cholesterol to disrupt lipid raft functions, EGFR behavior was affected[23]. Also, knockdown of clathrin, which is involved in endocytosis, using siRNA decreased the immobile fraction of EGFR[24].

These findings suggest that EGFR behavior is influenced by the molecular structure and membrane compositions. Therefore, the application of single-molecule imaging in drug discovery could allow for the detection of compounds that affect various factors related to the EGFR signaling. In particular, changes in the molecular diffusion and oligomerization, which are difficult to measure using conventional biochemical assays, can be referred as novel indicators of EGFR activity, offering a new avenue for drug evaluation methodologies.

Fig1.4

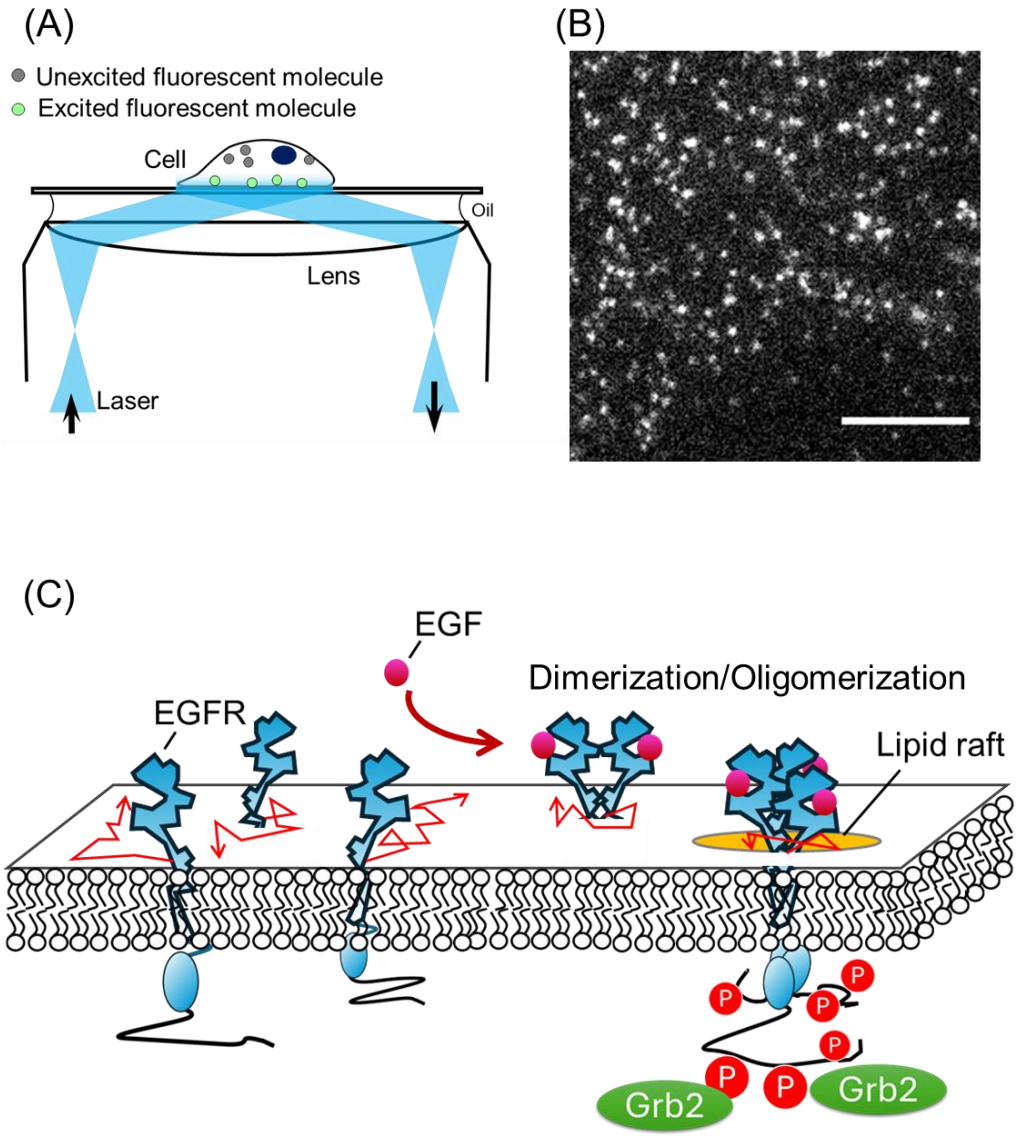

Fig. 1.4 Single-Molecule Imaging of EGFR

(A) A schematic diagram of total internal reflection fluorescence microscopy (TIRFM). The evanescent light illuminating ~150 nm thickness from the interface excites only the fluorescent molecules close to the cell membrane. (B) Single-molecule imaging of EGFR-mEGFP expressed in CHO-K1 cells. Scale bar, 5 μm. (C) Typical EGFR behaviors on the cell membrane. Red lines represent EGFR trajectories. The red circles represent phosphorylation (P), while the green circles indicate the downstream signaling molecule Grb2, which binds to the phosphorylated sites.

1.3 High throughput single molecule imaging

Conventional single-molecule imaging has been carried out manually, therefore, it relies heavily on specialized expertise and manual workflows, especially focusing with high magnification objective lens, searching cells suitable for single-molecule imaging, and adding drug solutions. This limitation has hindered its application to large-scale and high-throughput analysis. To address this issue, a fully automated intracellular single-molecule imaging system, AiSIS (Automated in-cell Single-molecule Imaging System), equipped with a novel automatic focusing device, machine learning for cell searching, and dispensing robotics, was developed[25].

This innovation increased the throughput by 100 times compared to the manual operation, enabling a large-scale analysis such as screening for compounds those affect the diffusion and oligomerization of fluorescently labeled membrane proteins. AiSIS has a potential to be a powerful tool for drug exploration.

Fig1.5

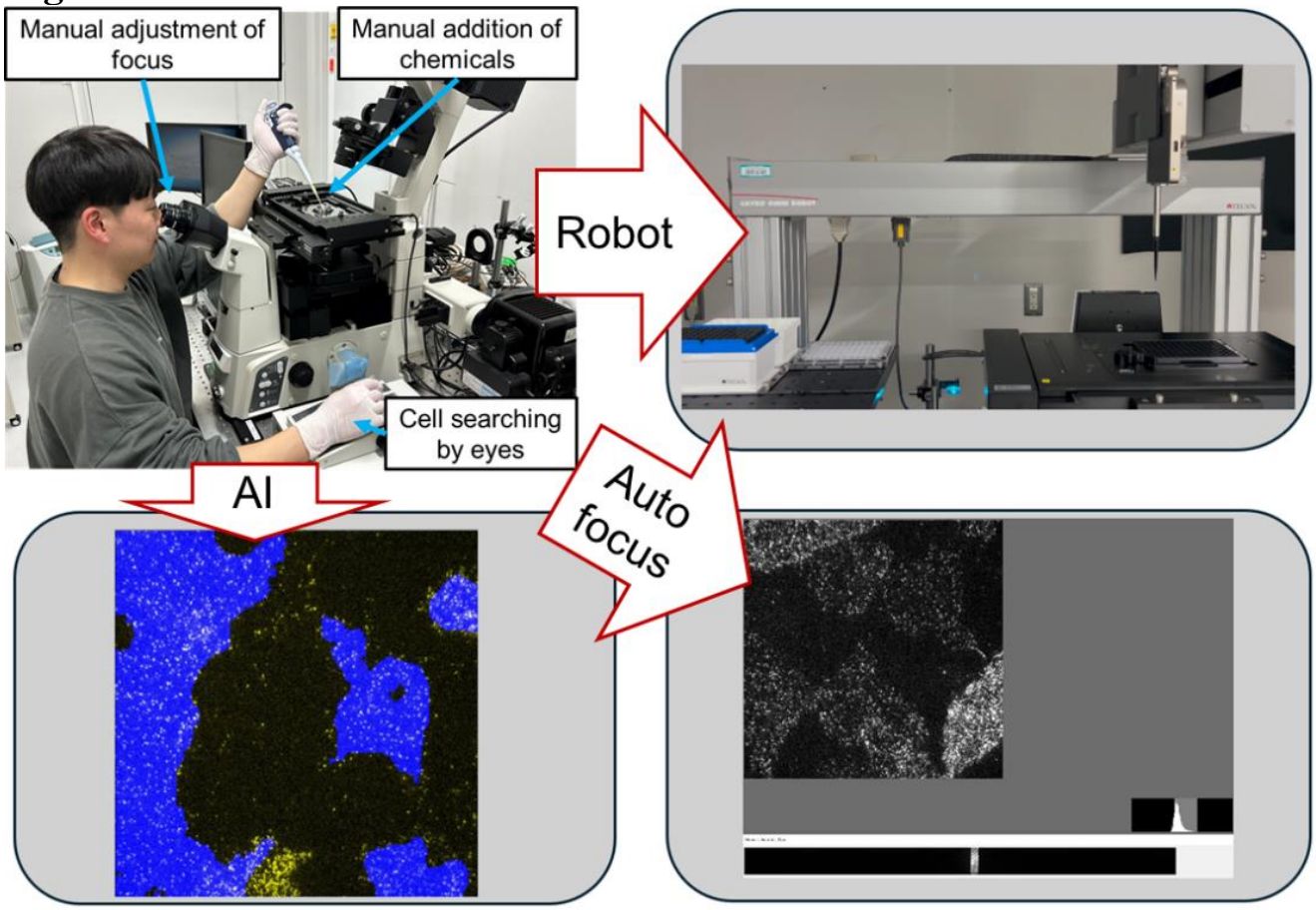

Fig. 1.5 Automation of single-molecule imaging

(Upper left) Manual single-molecule imaging process. (Upper right) Drug addition using a robotic arm with pipette. Drug is sucked up and added into the well. (Bottom left) Cell searching process using AI. The blue regions indicate areas recognized by AI as suitable regions for single-molecule tracking. Image acquisition is executed until the number of images reaches the desired number. (Bottom right) Focus adjustment sufficient for single-molecule imaging. A new autofocus system uses a slit-based principle described in the method section.

1.5 Results summary

In this study, I evaluated the utility of large-scale single-molecule imaging by an automated system as a method for drug screening. I targeted EGFR, for which numerous drugs have already been approved, and screened 1,134 known compounds including EGFR tyrosine kinase inhibitors with the information about diffusion and oligomerization of EGFR.

The screening selected three types of compounds affecting EGFR behavior: 1. compounds that suppressed the EGF-induced decrease in the mobility, 2. compounds that decreased the mobility regardless of EGF, and 3. compounds that inhibited the oligomerization. Among them, all the compounds that suppressed EGF-induced reduction in diffusion range were known as EGFR inhibitors, demonstrating the validity of the screening method. The other two types of compounds were previously unrecognized as EGFR tyrosine kinase inhibitors. These compounds were shown to reduce cell viability only in cells expressing EGFR. Additionally, they contributed to EGFR internalization. These findings indicate that single-molecule screening can identify drugs that act on multiple steps in signal transduction beyond phosphorylation. The EGFR phosphorylation has been referred in the conventional and primary screenings. My method using the additional information enables the discovery of novel drugs effective against receptors through previously uncharacterized mechanisms of action.

Chapter 2

Materials and Methods

2.1 Materials

2.1.1 Cell lines

The cell lines used in the study are summarized in the list below (Table 2.1). All cells were cultured in a 37°C CO2 incubator. CHOK1 parent strain was cultured in Ham's F-12 (05910, Nissui) 10% FBS medium. A431 and Hela cells were cultured in DMEM (FUJIFILM Wako Pure Chemical, Japan) 10% FBS. Ba/F3 parent strain were cultured in RPMI medium supplemented with 4 ng/mL IL-3 (091-03971, Fuji-Wako, Japan). Ba/F3-EGFR cells were additionally cultured with 20 ng/mL EGF (315-09, PeproTech, USA).

Table 2.1 Cell line

Strain name	Background	Source
CHOK1	CHO-K1	RIKEN BRC
CHOK1-EGFR-mEGFP	CHO-K1	This study
A431	A431	RIKEN BRC
Hela	Hela	RIKEN BRC
Ba/F3	Ba/F3	RIKEN BRC
Ba/F3-EGFR	Ba/F3	from Dr. Ryo Iwamoto and Dr. Eisuke Mekata, Osaka University

2.1.2 Cell preparation for single molecule imaging

EGFR-mEGFP was transfected into CHOK1 cells with FuGENE® HD Transfection Reagent (Promega, USA). Two or three days later, a population of cells exhibiting mEGFP fluorescence was collected using the CellSorter (Sony SH800S, Japan) with a 488 nm laser. This cell population was then cloned using the limiting dilution method. After cultivating the clones, cells were seeded in a 96-well plate (GP96000. Matsunami Glass, Japan), and the expression levels of EGFR-mEGFP were observed in each clone using total internal reflection fluorescence microscopy. Clones stably expressing an average of 0.76 ± 0.55 molecules per μm^2 were selected. In the actual measurements, AI was used to identify and observe cells with expression levels suitable for observation.

2.1.3 Compounds

The compounds used for drug screening were sourced from the Graduate School of Pharmaceutical Sciences and consisted of The Library of FDA-approved Compounds"(Selleck Chemicals, USA). The compounds were dissolved in DMSO at a concentration of 10 μM and diluted with DMEM for use. Negative controls consisted of DMSO (Wako; 043-07216), and positive controls used 10 μM gefitinib(Wako; 078-06561),which was diluted with DMEM according to the experimental conditions.

2.2 Methods

2.1.1 Automated in-cell single-molecule imaging system (AiSIS)

The total internal reflection fluorescence (TIRF) microscope was constructed by equipping a laboratory-made TIRF system with a microscope (Ti2-E, Nikon, Japan), as detailed in Figure 2.1. A 488 nm wavelength laser was used and directed at an angle to achieve total internal reflection through a 60× objective lens (PlanApo 60X NA 1.49, Nikon, Japan). The emitted fluorescence was passed through the dichroic mirror/emission filter set (DM495/BA500-545, Nikon, Japan) and detected using an sCMOS camera (ORCA-Flash4.0 V2, Hamamatsu, Japan).
For autofocus during single-molecule imaging, an autofocus unit (AIS, ZIDO Corp.) was utilized. A robotic arm (Cavro Omni Robot, Tecan, USA) was used to add 100 μL of EGF solution to the observation well. The stage control of the microscope, reagent addition, and focus adjustment were automated using AIS (ZIDO Corp.).

Table 2.2 TIRF microscope for single molecule imaging

Part name	Details
Housing	Ti-2E; Nikon
Objective lens	CFI Apo TIRF 60X Oil N.A 1.49; Nikon
Camera	ORCA-Flash4.0; HAMAMATSU
Laser	OBIS; COHERENT (output 488nm, 30mW)
Robot arm	Omni Robot (Tecan)
dichroic mirror/emission filter	DM495/BA500-545 (Nikon)

Fig2.1

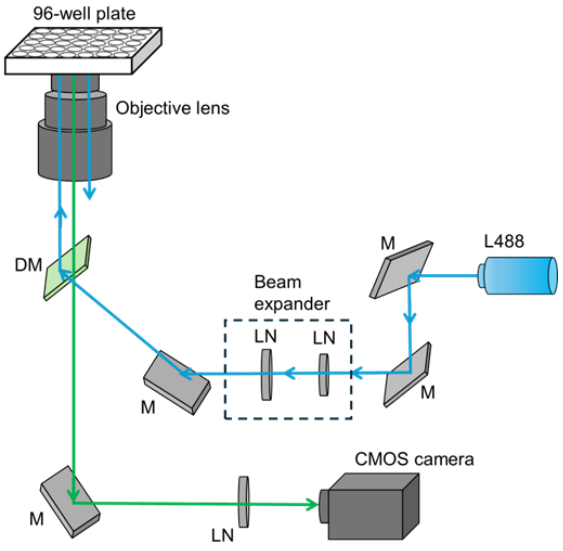

Fig. 2.1 Overview of the TIRF microscope

(A) Schematic Diagram of the Constructed Microscope

M: Mirror, DM: Dichroic Mirror, L: Lens. L1 and L2 are components inside the laser expander (SIGMA KOKI; LBED-10).

2.1.2 Autofocus devise

To achieve high precision autofocusing, an apparatus was set up consisting of a light source, a magnifying optical system, a slit, a CCD camera as a sensor for capturing the slit image, and a control unit for feedback control of the objective lens position. The light source emits an 830 nm wavelength laser, and a galvanometer mirror oscillating at 10 Hz directs the laser beam in two directions. The reflected light from the glass surface is detected by the sensor, enabling precise adjustments of the focal position.
The slit image detected by the CCD camera shifts according to the Z-axis position of the objective lens. When the slit image is centered, it indicates that the focus is correct. If the objective lens position is out of focus, the slit image shifts away from the center. Switching the light path using the galvanometer mirror causes the shifted slit image to appear on the opposite side of the center, relative to the initial position.
The difference in the positions of the two slit images corresponds to the displacement of the objective lens. By calculating the deviation from the center, the system can adjust to bring the focus position. When the slit image is centered, the edges of the slit image are detected by scanning the acquired image from one side and identifying the points that exceed a preset threshold. This threshold is configured to not detect if the slit is slightly blurred. Since the defocus offset D in the Z-direction translates to a focus adjustment of D/(square of magnification).this method enables high-precision autofocusing.

Fig2.2

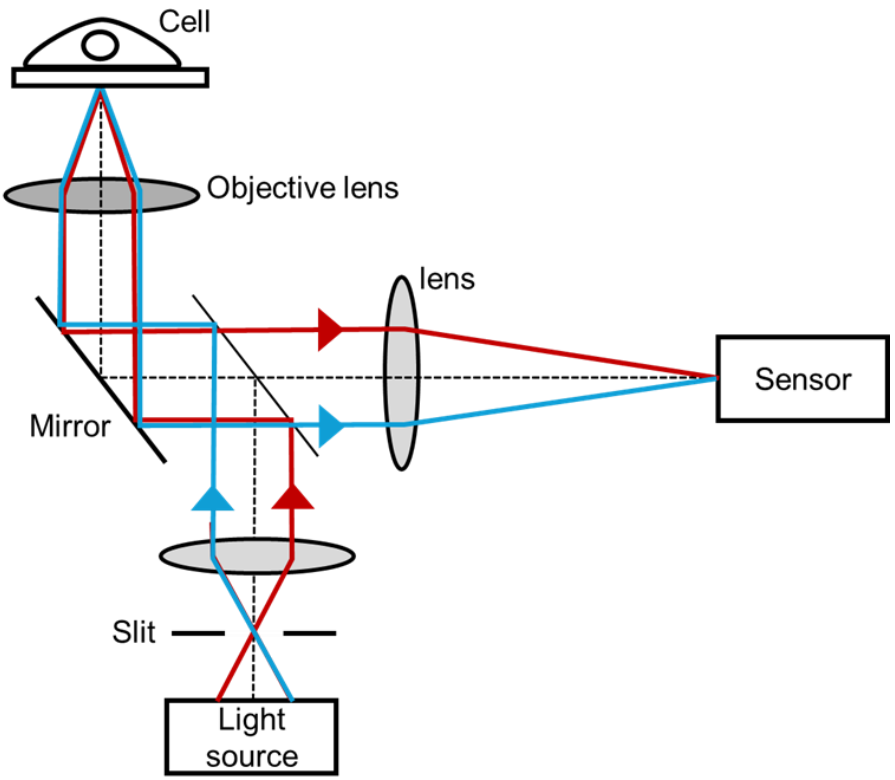

Fig. 2.2 Overview of the autofocus device

The illustration of the autofocus device. A laser with a wavelength of 830 nm is directed from two directions by galvanometer mirrors. The red and blue lines represent the two light paths. The sensor used is a CCD camera.

Fig2.3

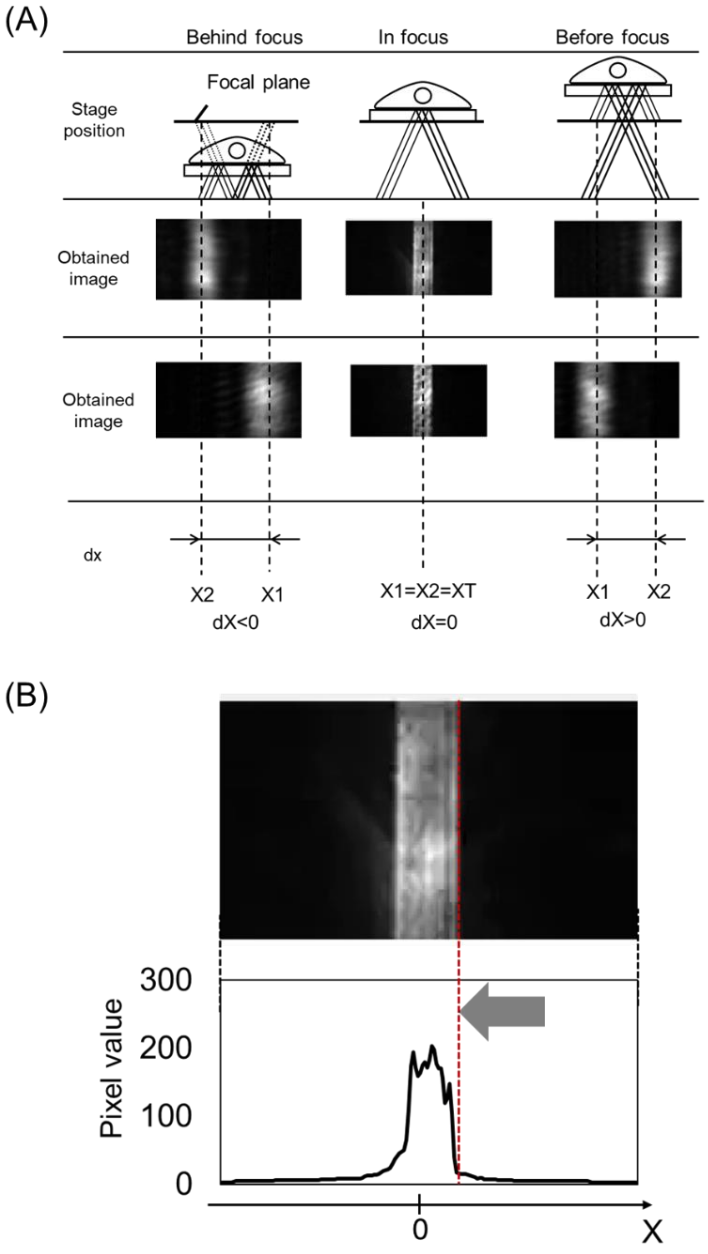

Fig. 2.3 Slit Images for realizing autofocus

(A) Relationship between the stage position and slit images detected by the camera. If out of focus, the slit image is detected at a position away from the center. When in focus, the image is detected at the center. (B) Mechanism of edge detection in the slit image. Arrows represent the scanning direction. Areas that exceed a threshold from one side are detected as edges.

2.1.3Single-molecule screening

For drug screening using single-molecule imaging, cells were seeded in 60 wells of a 96-well plate, excluding the outermost wells. Gefitinib was added to the wells on the leftmost side, DMSO to the rightmost wells, and 100 μL of 10 μM compounds was added to the remaining wells. The plate was incubated at 37°C in a CO_2 incubator for over an hour. For screening, 20 cells per well were observed both before and after EGF addition. After-EGF treatment data were obtained after adding 100 μL of 120 nM EGF to bacome a final concentration of 60 nM, followed by a 2-minute incubation before observation. To evaluate the screening accuracy for each plate, the Z'-factor was calculated.

$$Z' = 1 - \left(3 \times SD_{positive} + 3 \times SD_{negative}\right) / \left(Avg_{positive} - Avg_{negative}\right) \quad \text{(eq2.1)}$$

, where $SD_{positive}$, $SD_{negative}$, $Avg_{positive}$, and $Avg_{negative}$ represent the SD and average for the positive and negative controls, respectively. For the diffusion screening, MSD values from Gefitinib-treated wells were used as the positive control, and DMSO-treated wells as the negative control. For fluorescence intensity screening, EGF-treated wells served as the positive control, and DMSO-treated wells as the negative control.

2.1.4 Cell viability assay

Cells were initially seeded in 96-well plates (1860-096, Iwaki, Japan). These cells were incubated until reaching 90% confluence at 37°C in a CO2 incubator. Subsequently, the medium was replaced with compounds at a concentration of 10μM. For the measurement of Ba/F3-EGFR, EGF at 20ng/ml was added. After the incubation for 72 hours, I used the Cell Counting Kit-8 (Dojindo, Japan) to measure cell growth,. Following a 2-hour incubation, the absorption of the medium was measured at a wavelength of 450 nm using a plate reader (Infinite F50 Plus, Tecan, US).

2.1.5 Western blotting

To prepare cell lysates I used a sample buffer containing SDS. The lysates were loaded onto a 10% SDS-polyacrylamide precast gel (192-14961, SuperSep Ace, 10%, 17 wells, FUJIFILM Wako Pure Chemical, Japan) and electrophoresed at 300V. Proteins from the gel were transferred on a ClearTrans PVDF Membrane (Hydrophobic, 0.45 μm, FUJIFILM Wako Pure Chemical, Japan). The membrane was blocked with 2.5% skim milk and then incubated overnight with primary antibodies specific to the target proteins, followed by HRP-conjugated secondary antibodies for 1hour RT. Detection of HRP activity was performed using the ECL Prime reagent (Cytiva, USA).

Table 2.2 Reagents list for western blotting

4×Sample buffer	Tris HCL (pH6.8) 1M	10 mL
	70% Glycerol	14.3 mL
	20% SDS	10 mL
	β-ME 14M	7.15 mL
	EDTA 0.5M	0.4 mL
	BTB	0.1 g
	miiliQ	Up to 50 mL
10×SDS buffer	Tris(25mM)	30 g
	Glycine(0.1M)	144 g
	SDS(0.1%)	10 g
	miiliQ	Up to 1 L
TBS-T (Wash buffer)	Tris (pH7.5)	20 mM
	NaCl	137 mM
	Tween-20	0.05%
Transfer buffer	Glycine(192mM)	43.2 g
	Tris-base(25mM)	9.1 g
	MeOH(15%)	450 mL
	miliQ	Up to 3 L
2.5% Skim milk	Skim milk (nacalai tesque, 31149-75)	2.5 g
	TBS-T	Up to 100 mL

2.1.6 Internalization assay

To evaluate internalization, the intensity of fluorescent spots on the cell membrane was measured using total internal reflection fluorescence (TIRF) microscopy. CHO-K1 cells were treated with compounds, and images of the same cells were captured at 10-minute intervals after drug treatment. For Verteporfin treatment, due to its photophysical effects, measurements were taken at 20-minute intervals. The obtained images were analyzed by enclosing the intracellular area with a circle, subtracting the fluorescence intensity outside as a background.

2.1.7 Fluorescent immunostaining

Cells cultured on glass-bottom dishes were treated with 10 μM of compound for 1 hour, fixed with 4% PFA at -30°C for 30 minutes, and washed with HBSS. The cells were then permeabilized with Triton X-100 in HBSS and blocked with HBSS containing 2% BSA for 15 minutes. Subsequently, the samples were incubated with the primary 1:300 dilluted anti-EGFR antibody (#4267, CST, USA) or 1:10,000-diluted anti-caveolin antibody (#3267 T, CST, USA) at room temperature for 1 hour. After three washes with HBSS, the samples were incubated with a secondary anti-IgG antibody conjugated with Alexa 488 or Alexa 647 (#A-11034 or #A-21244, respectively, Invitrogen, USA) for 1 hour. Nuclear staining was performed using 0.05% NucSpot Live 650 (Biotium, USA) for 30 minutes. The samples were observed using a confocal microscope system (Nikon A1) with a 20× objective lens, exciting at the corresponding wavelengths.

2.2 Analysis

2.2.1 Single-molecule tracking

Single-particle spot recognition and trajectory acquisition were performed using Auto Analysis Software (AAS, ZIDO, Japan) for obtain position of spot followed by this formula.

$$I(x, y; I_0, x_g, y_g, \sigma_x, \sigma_y, a, b, I_{back})$$

$$= I_0 \exp\left[-\frac{(x-x_g)^2+(y-y_g)^2}{2\sigma_x\sigma_y}\right] + a(x - x_g) + b(y - y_g) + I_{back} \qquad \text{(eq2.2)}$$

The x and y indicate the position of spot. The bright spot fitted to the equation for the plane with the background slope a, b and intercept I_{back} is added to the Gaussian function with the center x_g, y_g standard deviation sigmax, sigmay and peak I_0.

After CHOK1-mEGFP image was captured using a total internal reflection fluorescence microscope, the cell regions were determined using AI, followed by trajectory tracking. The parameters used for analysis were as follows: ROI size: 6, scan size: 3, intensity threshold: 10, and maximum distance: 8.

Fig2.4

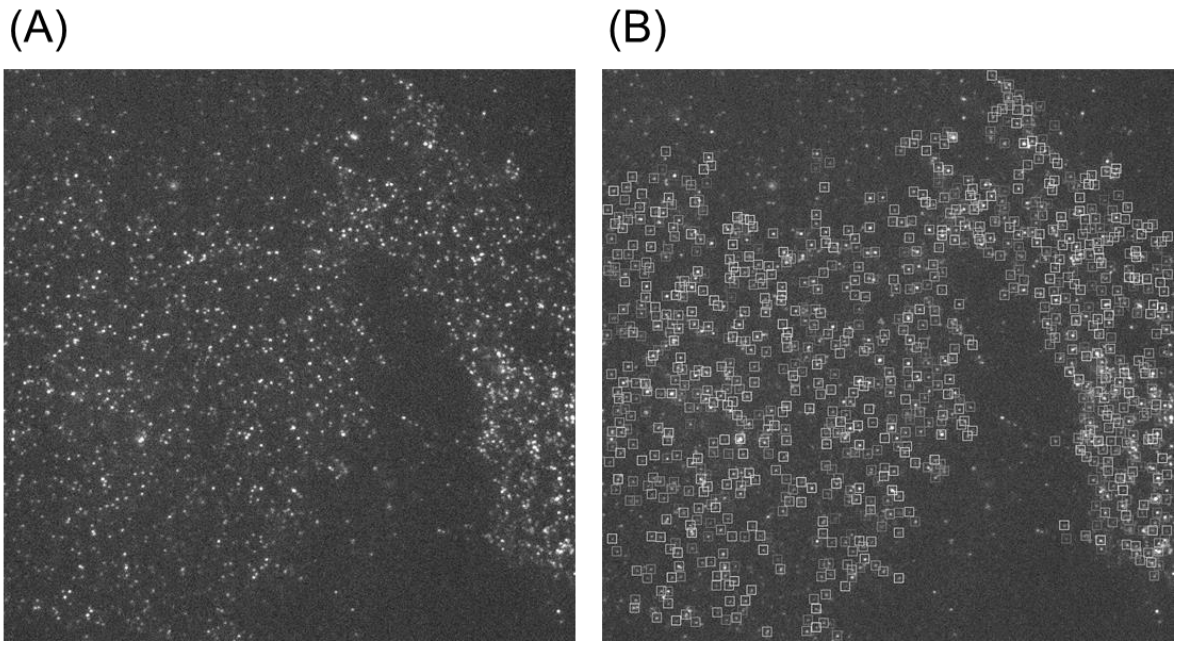

Fig. 2.4 Recognition of single particle spots

(A) Images taken using total internal reflection fluorescence microscopy (TIRFM) with CHOK1 cells expressing EGFR-mEGFP. (B) Recognition applied to the image in (A) using Automated Analysis System (AAS). The bright spots enclosed in boxes represent recognized points.

2.2.2 Mean squared displacement

To quantify the diffusion range from the obtained single-molecule trajectories, the mean squared displacement (MSD) was calculated using the following equation:

$$MSD(n\Delta t) = \{[x_i\text{-}n\Delta t + m\Delta t - x_i(m\Delta t)]^2 + [y_i(n\Delta t + m\Delta t) - y_i(m\Delta t)]^2\}_{i,m} \cdot \quad \text{(eq2.3)}$$

The variables x and y represent the XY coordinates of the fluorescence spot, n,m denote specific frame numbers, and i indicate the trajectory number. [] indicate averaging over all relevant indices. Δt refers to the frame rate, which was 33 ms in this measurement.

The concentration-dependent fitting using MSD was performed based on the following equation:

$$MSD = MSD_{max} - \frac{MSD_{max} - MSD_{min}}{1 + (\frac{EC_{50}}{[I]})^h} \quad \text{(eq2.4)}$$

For fitting the mean square displacement (MSD) in a 2D plane, the following equation based on the noncompetitive inhibition.

$$MSD = MSD_{max} - \frac{MSD_{max} - MSD_{min}}{(1 + (\frac{EC_{50}}{[L]})\ )(1 + (\frac{[I]}{IC50})\ )} \quad \text{(eq2.5)}$$

2.2.3 Quantification of EGFR internalization

To quantify the total amount of EGFR and its internalization, images obtained from fluorescence immunostaining were analyzed. After detected the cells using Cellpose 3.0[26], [27], [28], the area 5 pixels outward from the identified cell boundary was used as the cell membrane, while the excluding the nucleus and cell membrane was intracellular region.. Background subtraction was applied, and the extent of internalization was calculated using the following formula:

$$I_{mem}/I_{cyt} = (F_{mem} - F_{bck})/(F_{cyt} - F_{bck}), \qquad \text{(eq2.6)}$$

F_{mem} indicates the average fluorescence intensities of the plasma membrane, F_{cyt} indicates the average fluorescence intensities of the cytoplasm. To quantify both internalization and degradation, the total fluorescence intensity of the cell was measured, and the following formula was applied:

$$\alpha \cdot I_{mem}/I_{cyt.}, \qquad \text{(eq2.7)}$$

α indicates the the average fluorescence intensity of the whole cell except for nuclei. This calculation could evaluate EGFR internalization and degradation, based on fluorescence intensity distributions.

Chapter 3

Results

3.1.1 EGFR mobility-related EGFR activation

Single-molecule imaging enables direct visualization of individual fluorescently-labeled molecules, allowing the measurement of their positions and fluorescence intensities. By single-molecule imaging on fluorescently labeling EGFR, it has been shown that the mean squared displacement (MSD) of EGFR trajectories which corresponds to the diffusion range, decreases upon the binding of EGF.

To confirm whether this change is associated with signaling processes, the relationship between diffusion range and phosphorylation, one of the steps in the EGFR signaling cascade, was examined. As the results, the MSD at a duration time of 500 ms decreased in an EGF dose-dependent manner. The EGF dose-dependent phosphorylation levels of EGFR measured using Western blot analysis was shown to increase.

The half-maximal effective concentrations (EC_{50}) for the two measurements were 2.1 nM for MSD and 1.5 nM for phosphorylation, showing a linear relationship between the mobility and phosphorylation.

These results suggest that the decrease in the EGFR mobility observed in single-molecule imaging reflected the EGFR phosphorylation process, enabling to utilize the mobility for quantification of the EGFR activation.

Fig3.1.1

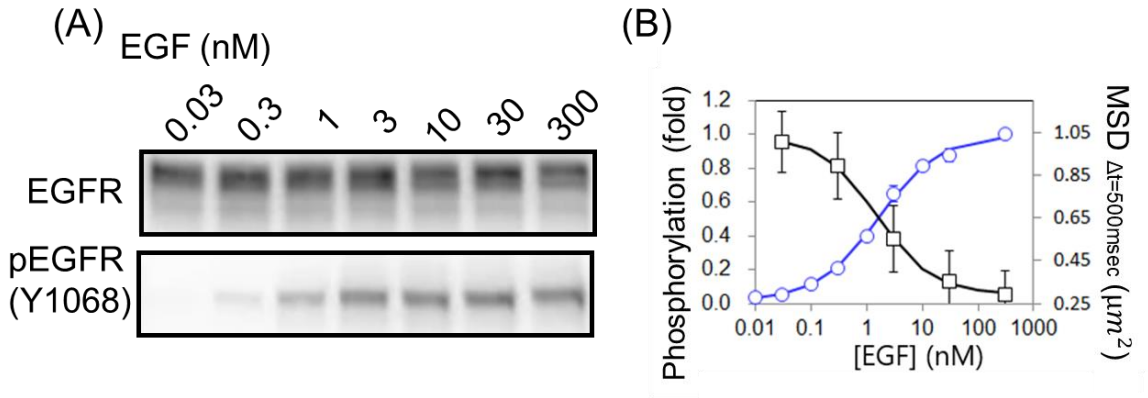

Fig. 3.1.1 EGFR phosphorylation correlates with MSD

(A) Measurement of phosphorylated EGFR using Western blotting. (B) Blue circles: Quantification results of western blot results. Black boxes: Mean Square Displacement (MSD) representing the MSD at Δt= 500 ms of EGFR diffusion. The curves represent the fitting results for each. The EC_{50} value is 2.1 nM for phosphorylation, and 1.5 nM for MSD results, indicating a correlation between EGFR phosphorylation and mobility.

3.1.2 EGFR mobility can estimate inhibitory effects of drug

To assess whether EGFR phosphorylation inhibitors can be evaluated using single-molecule analysis, I conducted the experiments to obtain MSD of wild-type (wt) EGFR and EGFR with a single mutation (L858R) under various concentrations of gefitinib, a tyrosine kinase inhibitor (TKI) of EGFR, and EGF (Fig3.1.2). At lower concentrations of gefitinib, EGF induced dose-dependent decrease in the MSD. However, at higher concentrations, this EGF-dependent decrease in the MSD was weak in both types of EGFR.

By fitting the experimental data to a non-competitive inhibition model, the IC_{50} value of gefitinib for the MSD of wt EGFR was determined to be 8.9 μM (Fig3.1.2A), which is close to the previously reported values obtained by cell biochemical method [29]. Additionally, when the same measurements were performed for the gefitinib-sensitive L858R mutant, the IC_{50} was calculated to be 0.02 μM (Fig3.1.2B) that is also consistent with the previous study [30].

These results indicate that the inhibition by gefitinib can be precisely and effectively assessed by focusing on EGFR mobility observed by single-molecule imaging, suggesting that the method can be provided as a tool for evaluating kinase inhibitors like the traditional phosphorylation assays. Furthermore, the method demonstrated the ability to discriminate the inhibitory effect of gefitinib against wt and mutant EGFR.

Fig3.1.2

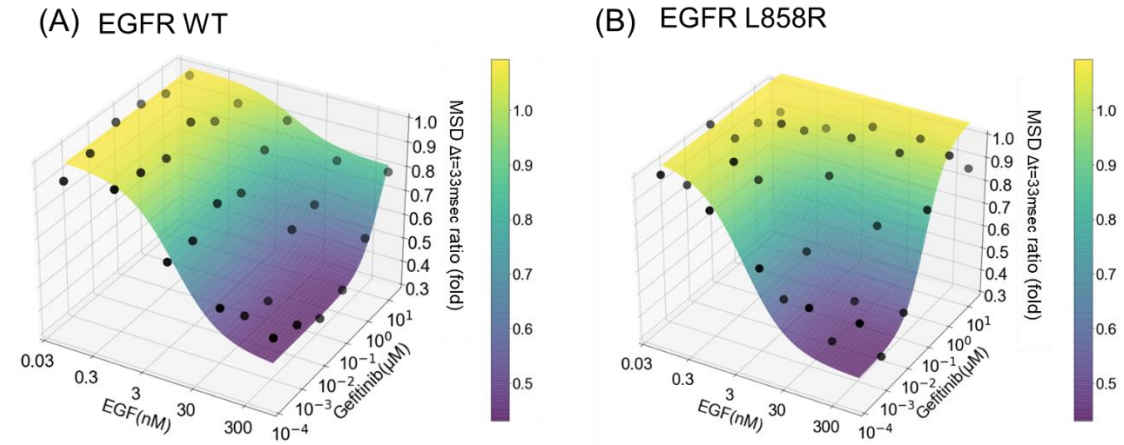

Fig. 3.1.2 The inhibition of kinase activity was evaluated based on the dose dependence of EGF and phosphorylation inhibitors.

For each panel, the X-, Y-, and Z-axis represent EGF concentration, the concentration of phosphorylation inhibitors, and the ratio of changes in MSD before and after EGF addition, respectively. The points represent the obtained ratio of MSDs at Δt = 500 ms before and after EGF addition. The fitted results with non-competitive inhibition model are represented by the colored surfaces. The obtained data and fitted surfaces were shown for (A) EGFR WT with IC_{50} of 8.8 μM and for (B) EGFR L858R with IC_{50} of 0.02 μM.

3.2 Single molecule tracking based drug screening

3.2.1 Validation of the screening method

Based on the experimental results, the effect of kinase inhibitors has been shown to be evaluated by focusing on the mobility. To extendedly apply the method to drug screening, I optimized the experimental condition of single-molecule imaging. When high-throughput screening (HTS) is performed in the primary screening, the assay for each compound is conducted only once, therefore, it is needed to establish conditions enabling a highly stable assay. The Z'-factor [31] is a widely used key index for evaluating the quality of drug screening. A screening assay with a Z'-factor greater than 0.5 is considered to be usable. To determine the minimum number of cells to satisfy the criterion in single-molecule imaging, I examined various sample sets with different number of cells. 600 cells treated with DMSO or gefitinib were respectively negative or positive control and measured before and after EGF stimulation. Distributions of MSD were calculated, and its probability density distribution was obtained (Fig. 3.2.1A). I referred the relationship between the number of sampled cells and Z'-factors calculated from MSD ratio between before and after EGF stimulation for each plate. The results showed that sampling at least 20 cells each before and after EGF addition ensures that more than 80% of the plates achieve the Z'-factor exceeding 0.5 (Fig. 3.2.1B).

Next, I measured the time for image acquisition. The results indicated there is a relationship between the number of observed cells and the measurement time (Fig. 3.2.1C). To minimize measurement time and maintain high accuracy, I decided to measure 20 cells per well. Under these conditions, I validated the Z'-factor every plate in which negative and positive controls were arranged as shown in the figure (Fig. 3.2.2A). I confirmed that the Z'-factor from all 5 plates consistently exceeded 0.5 (Fig. 3.2.2B). Additionally, the signal intensity (SB ratio), as well as the coefficient of variation (CV) values, met the respective criteria of SB ratio ≥ 2 and CV < 0.1. In these experiments, MSD at the Δt that maximized the Z' factor was calculated

Fig3.2.1

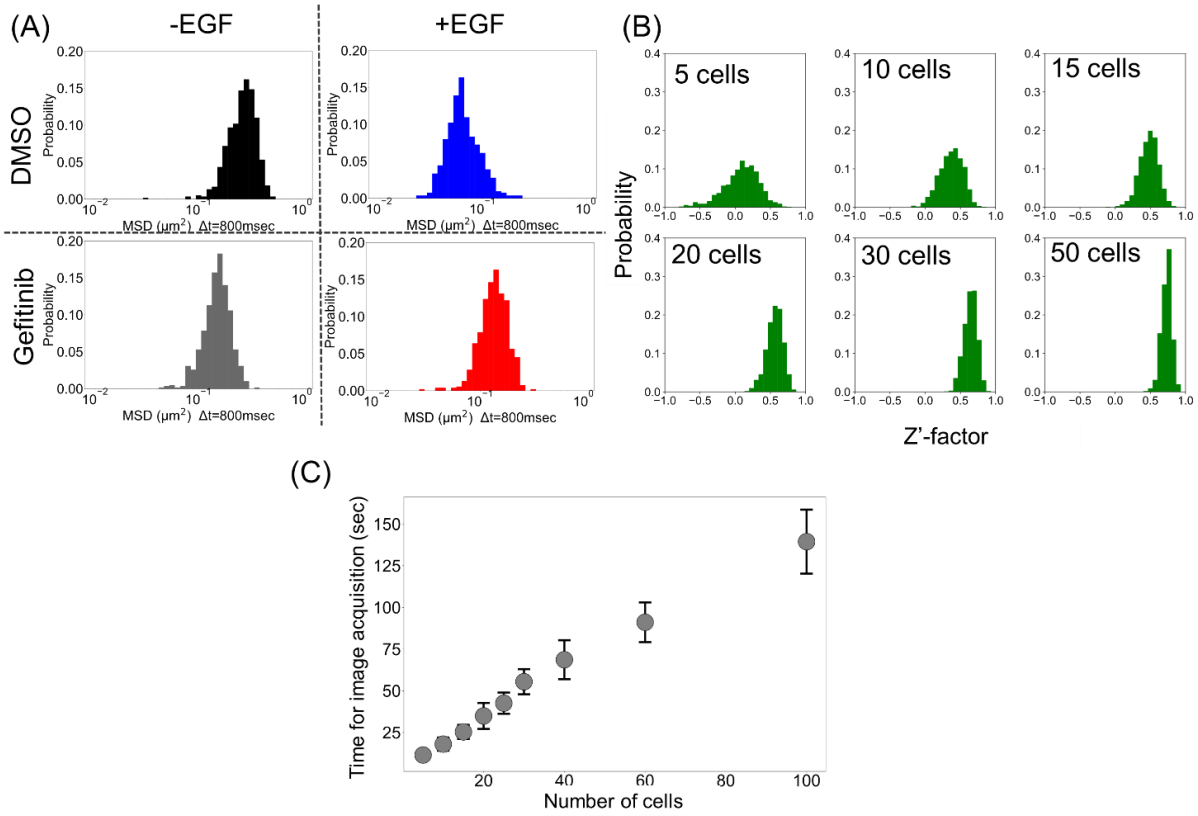

Fig. 3.2.1 Optimization of conditions for drug screening using single molecule imaging

(A) Histograms of MSD at Δt = 800 ms after EGF stimulation. DMSO was negative control and gefitinib (10 μM) was positive control. Data was obtained from 600 cells for each condition. (B) Z'-factor histograms calculated using MSD data randomly selected from the probability density distribution in (A). The Z'-factor was calculated based on the ratio of MSD values before and after EGF stimulation. Wells with DMSO was the negative control and those with gefitinib was the positive control. Sampling was performed from 1,000 different plates for each specified number of cells. (C) Measurement time required for different numbers of cells. Data represents the mean ± SD from five independent experiments.

Fig3.2.2

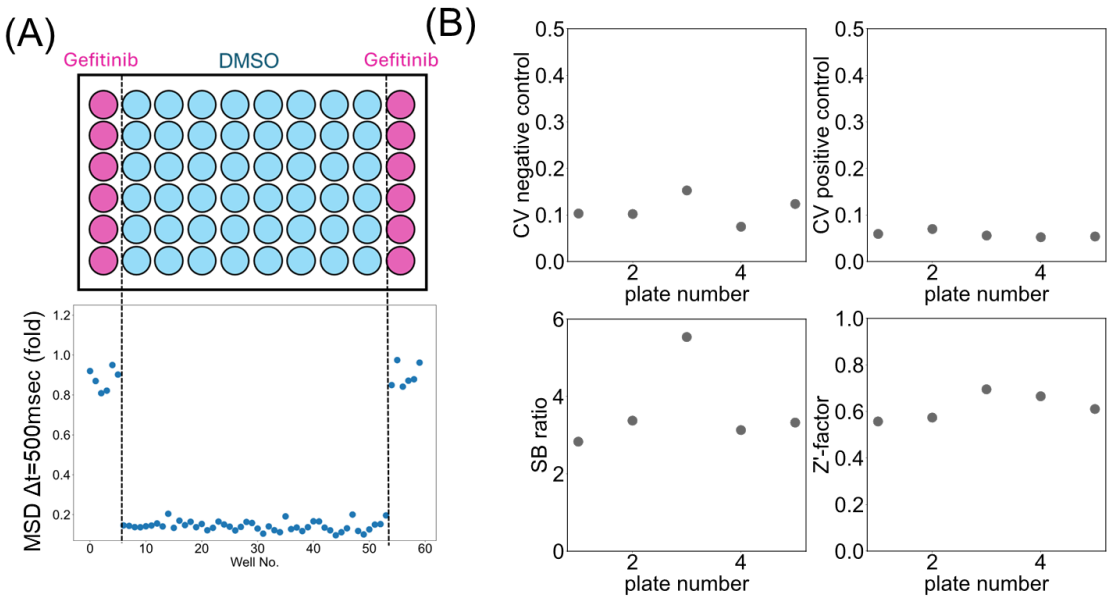

Fig. 3.2.2 Validation of drug screening using single-molecule imaging

(A) Schematic representation of a 96-well plate layout excluding the outer wells. Wells with DMSO were the negative control and those with 10 μM gefitinib were the positive control distributed across 60 wells. For each well, 20 cells were measured before and after EGF stimulation, and the ratio of MSD at Δt=500 msec was calculated. The negative control (DMSO) showed a decreased ratio after EGF stimulation, while the positive control (gefitinib) exhibited a higher ratio due to the inhibition of phosphorylation. (B) Screening metrics including the Z'-factor, SB ratio, and CV value were calculated across 5 plates. The results met criteria: Z'-factor ≥ 0.5, SB ratio ≥ 2, and CV value < 0.1.

3.2.3 Diffusion-based drug screening

To validate the utility of the single-molecule tracking-based screening I conducted a screening using a library of 1,134 FDA-approved compounds targeting a wide range of protein classes, including receptors, channels, kinases, enzymes, and transporters (Fig3.2.3). This library includes 7 drugs known to act as tyrosine kinase inhibitors (TKIs) against EGFR: afatinib, erlotinib, OSI-420 (the active metabolite of erlotinib), gefitinib, lapatinib, lapatinib ditosylate (an alternate form of lapatinib), and vandetanib. The applicability of screening could be evaluated by whether all known EGFR phosphorylation inhibitors were detected. If the system successfully identifies these compounds, it confirmed that the single-molecule imaging-based platform was applicable as an effective tool for screening of EGFR inhibitors.

Fig3.2.3

Target	Number of compounds	Proportion
Membrane receptors	207	21.9%
Enzymes	155	16.5%
Ion channels	67	7.1%
Nuclear receptors	61	6.5%
Transporters	41	4.4%
Non receptor kinases	10	1.1%
Cytokines	4	0.4%
Others	397	42.1%
Total	942	100%

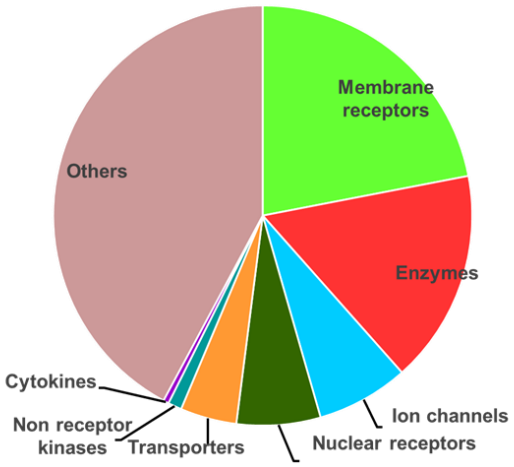

Fig. 3.2.3 Classification and proportions of compounds used in this study

Classification and proportions of molecules targeted by the 942 compounds in the library of 1134 FDA-approved drugs.

In a series of screenings using mobiity,1134 compounds were distributed in 24 plates. To check the quality of screening by using Z'-factor, wells with cells treated with negative control (DMSO) and positive control (gefitinib) were prepared in each plate. MSD at the Δt that maximized the Z' factor was calculated (Fig3.2.4). Further analyses were conducted only on the compounds contained in plates that exceeded the criterion of Z' > 0.5.

Fig3.2.4

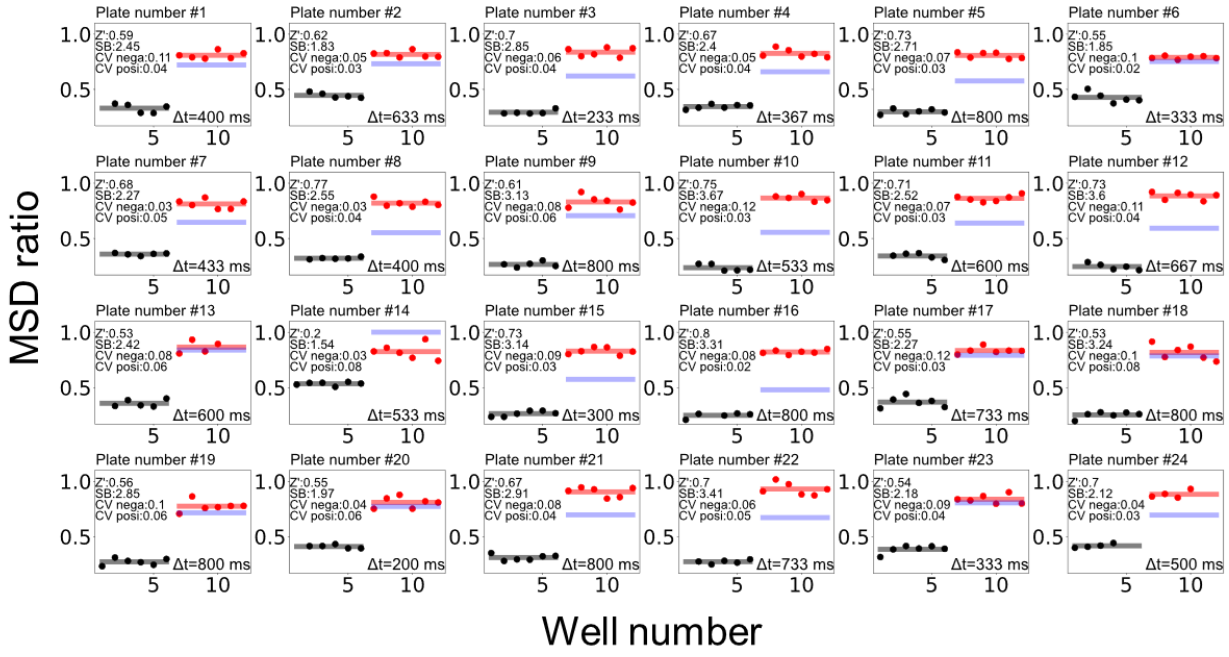

Fig. 3.2.4 Validation of drug screening based on diffusion

The plates used in the screening have positive controls (red dots for gefitinib) placed in the 6 wells and negative controls (black dots for DMSO) in the 6 wells. The red and black lines represent the average of each condition. The blue line shows values of Z'-factor exceeding 0.5 when the positive controls exhibit similar variability. The numbers at the lower right indicate the Δt which maximized the Z'-factor. The numbers in the upper corner represent the validation index for the plate as shown in order from top to bottom: Z'-factor, SB (Signal-to-Background) ratio, CV (Coefficient of Variation) for the negative control, and CV for the positive control.

In the screening, the ratio of MSD before and after EGF addition was measured for the cells treated with each compound. Hit compounds were selected as that the ratio exceeded the Mean ± 3 times the standard deviation of the negative control. As a result, 53 compounds were chosen(Fig3.2.5). Among them, genistein, which is known for EGFR inhibition but with an IC_{50} larger than 10 μM, was not screened in this process.

Fig3.2.5

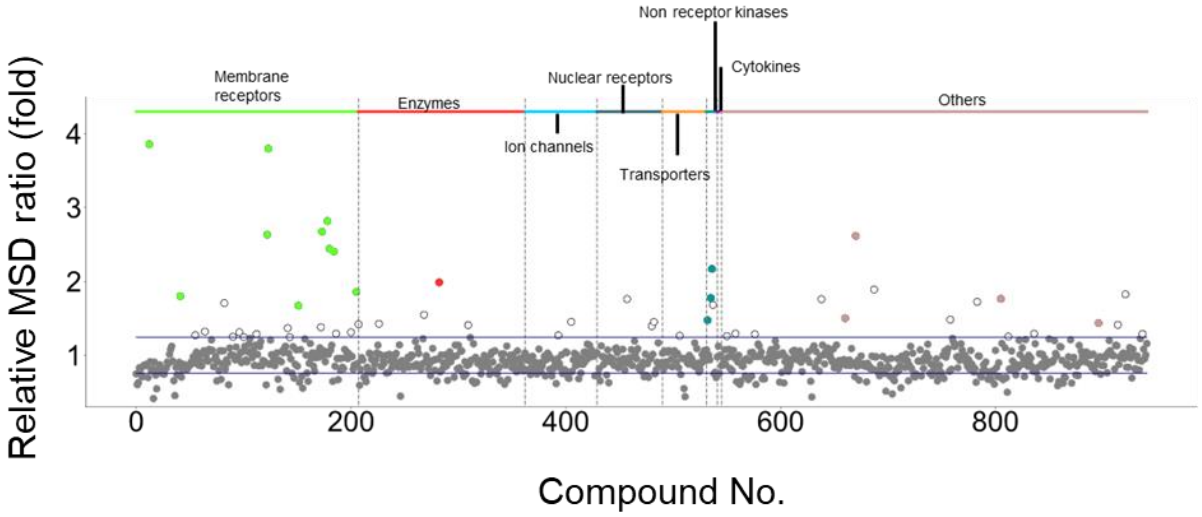

Fig. 3.2.5 Results of drug screening based on diffusion

The 942 compounds with the Z'-factor exceeding 0.5 were analyzed. The blue lines represent sum of the average of the negative control and mean value with adding (upper) or subtracting (lower) three-times of standard deviation of each well.. The colored and white circles indicate the 53 hit compounds that exceeded the threshold indicated by the upper blue line. The colored circles represent the 18 compounds selected by the further analysis (see below). Target proteins of compounds are shown above the bar.

Next, a dose-dependent test was performed on the 53 compounds obtained from the first screening. The MSD was quantified before and after EGF addition, with measurements taken from ~30 cells for each compound (Fig3.2.6).

Fig3.2.6

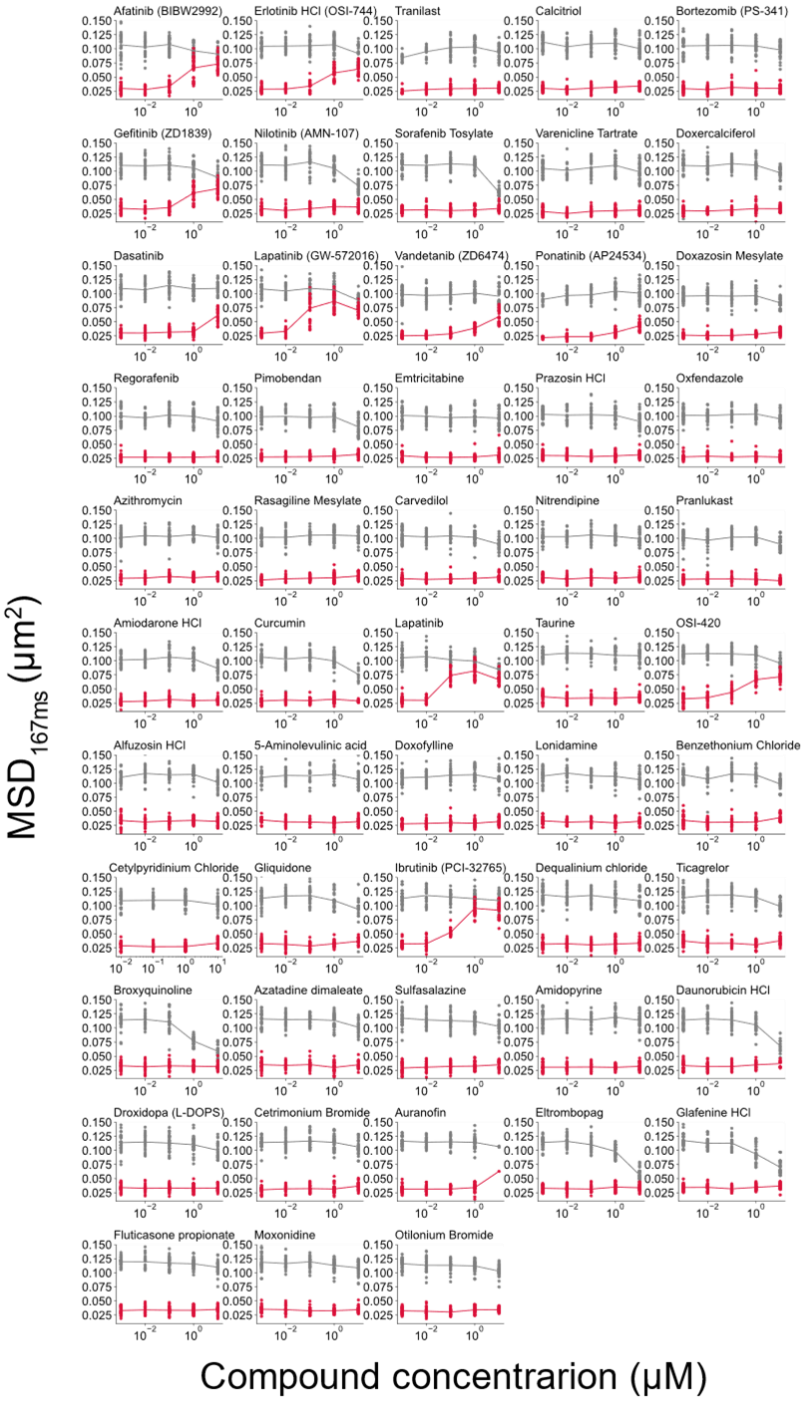

Fig. 3.2.6 Dose-dependent assay for 53 compounds from first screening

The dose-dependent assays for 53 compounds using single-molecule imaging. The x-axis in each graph represents the concentrations of the compound from 0.001 to 10 μM. Each point represents MSD value from one cell. Black and red dots indicate data before and after EGF addition, respectively.

From 53 compounds, I selected compounds exhibiting large differences in MSD between the minimum and maximum concentrations which exceeded half the standard deviation. As a result, 17 compounds except a cell-toxic compound, auranofin, were identified. Among them, 10 compounds didn't show a decrease in the MSD after EGF addition (Fig3.2.7A). On the other hand, the remaining 7 compounds uniquely exhibited the ability to reduce the MSD independently (Fig3.2.7B).

Fig3.2.7

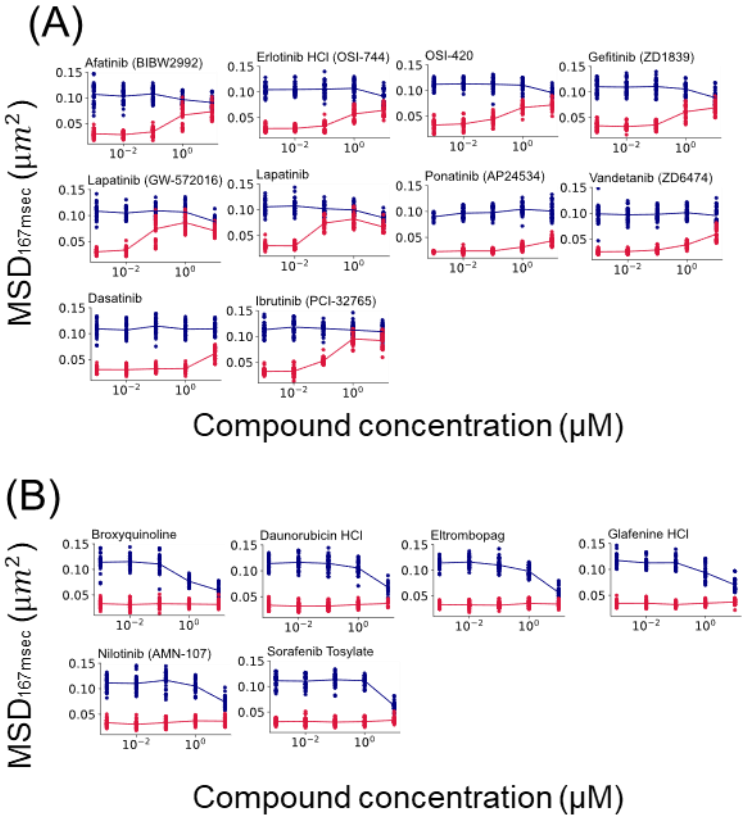

Fig. 3.2.7 Two types of compounds altering EGFR behavior in a dose-dependent manner

(A) Compounds increase MSD after EGF addition, demonstrating a dose-depency. (B) Compounds decrease MSD independent of EGF treatment, indicating a direct effect of the compound on EGFR behavior. Each dot represents a data from one cell. Blue and red dots represent before and after EGF stimulation respectively.

The compounds identified from the screening included Afatinib, Erlotinib, OSI-420, Gefitinib, Lapatinib, and Lapatinib ditosylate those are the EGFR-TKIs [9], [32]. Ponatinib, Vandetanib (pan-TKIs) [33], [34], Dasatinib, and Ibrutinib are those have been reported to inhibit EGFR phosphorylation [35]. This confirmed that all EGFR-TKIs from the library were successfully detected, suggesting that the method using single-molecule imaging for drug screening can detect inhibitors that bind to the ATP-binding pocket of EGFR, which have been discovered so far."

Among the other 7 hit compounds, Broxyquinoline, Daunorubicin, Eltrombopag, Grafinine, Nilotinib, Sorafenib have different indications and targets as follows (Table3.1).

Table 3.1 Drugs decreased MSD of EGFR

Compounds	Disease	Target
Broxyquinoline	Protozoan infection	infective agent[36]
Daunorubicin	Acute myeloid leukemia	DNA topoisomerase II[37]
Eltrombopag	Severe aplastic anemia	TPOR[38]
Glafenine	Inflammatory	COX-2/PGE2[39]
Nilotinib	Kidney cancer	Bcr-Abl tyrosine kinase[40]
Sorafenib	Chronic myeloid leukemia	Many protein kinases, including PDGFR, VEGFR and RAF kinases[41]

3.2.4 EGFR clustering-based screening

Oligomer formation is known to be associated with signaling efficiency and can be considered as an index for drug discovery. Single-molecule imaging allows for the measurement of fluorescence intensity, which reflects oligomer formation. Since CHO-K1 cells do not express endogenous EGFR, the brightness of a fluorescence spot of EGFR-mEGFP reflects the number of EGFR molecules involved in oligomer formation. Because oligomer formation was facilitated following EGF stimulation, an EGF concentration-dependent increase in the brighter fractions was analyzed (Fig3.2.8).

Fig3.2.8

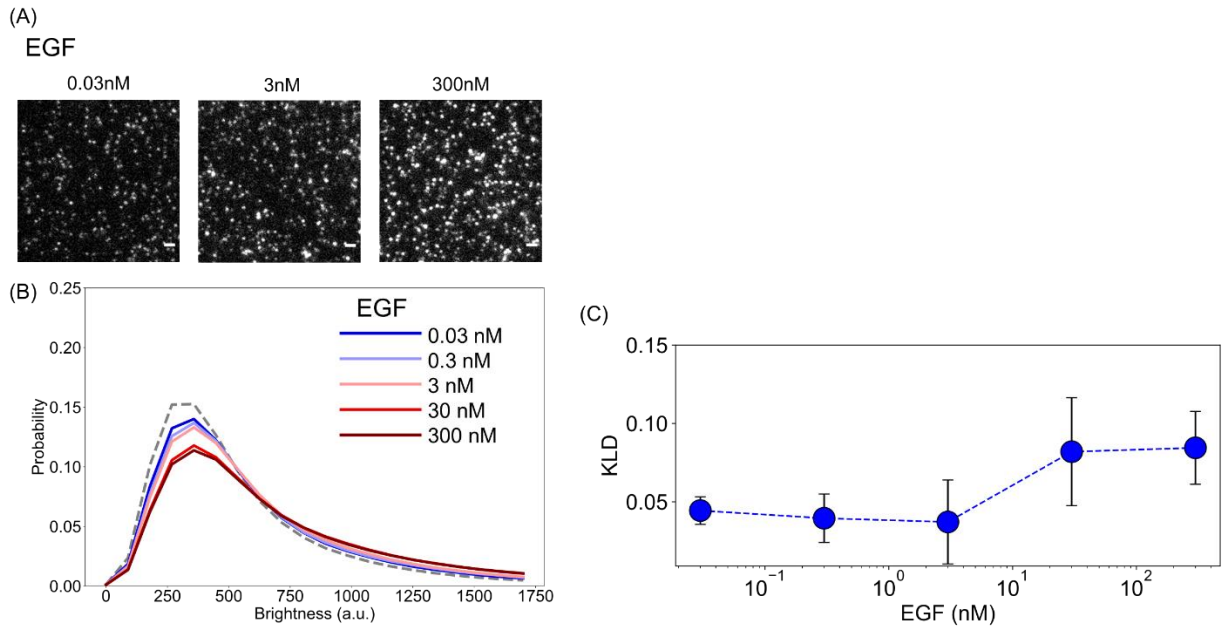

Fig. 3.2.8 Measurement of fluorescence intensity after EGF stimuli

(A) Images obtained from single-molecule imaging of CHO-K1 cells expressing EGFR-mEGFP with various EGF concentrations of 0.03 nM, 0.3 nM, and 300 nM at 2 minutes after the stimulation. Scale bar represents 5 μm. (B) Histograms of fluorescence intensity of the bright spots. Higher EGF concentrations resulted in increases in the brightness fraction. (C) The data represent KLD under conditions without EGF stimulation and with EGF stimulation at various concentrations. Data represents the mean ± SD from 4 independent experiments.

In the first screening where 1134 compounds were tested, the probability density distributions of fluorescence intensity were also obtained and compared to that of the DMSO control condition. For each compound, to quantify the deviation from the fluorescence intensity distribution under the DMSO condition, Kullback–Leibler Divergence (KLD) was used. The validation was performed for each plate under the EGF stimulation. Although increase in the fluorescence intensity was observed, none of the plates achieved the criteria of Z'-factor which exceeds 0.5 due to high CV values. (Fig3.2.9).

Fig3.2.9

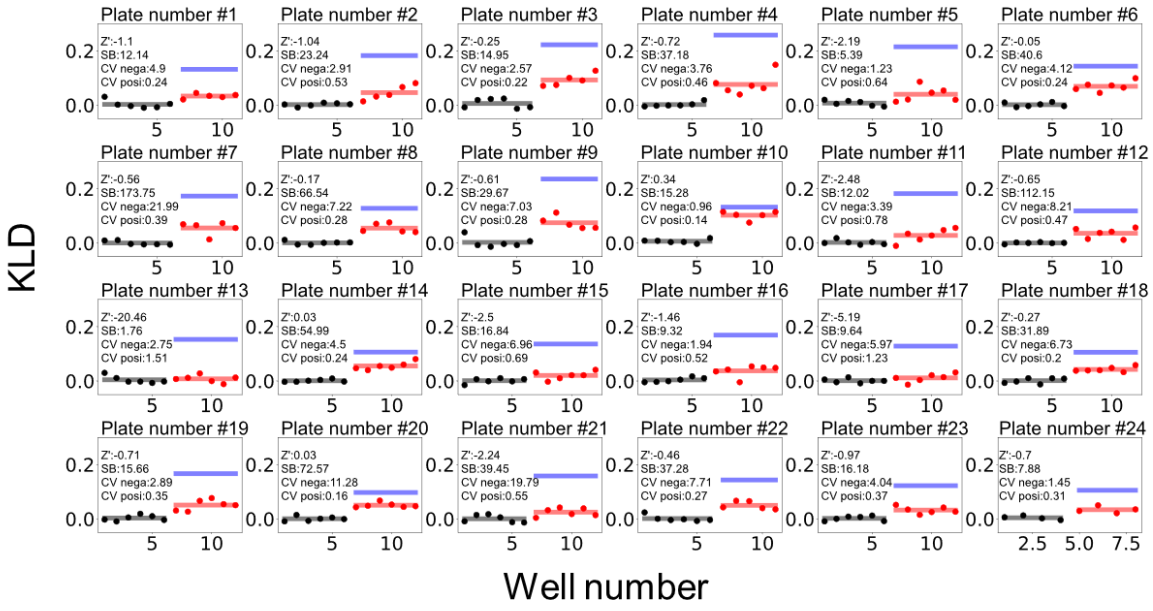

Fig. 3.2.9 Validation of drug screening using fluorescence intensity

The rightmost and leftmost 6 wells in a plate were used for the validation. Black dots represent the negative control (DMSO). Red dots represent the positive control, which was stimulated by EGF. Red and black lines denote the averages. Blue lines indicate the required average of the positive control to achieve a Z'-factor ≥ 0.50 , suitable for screening. This was calculated using the standard deviation of the positive and negative controls, along with the average of the negative control. The numbers in the upper right represent the validation index for the plate. Values in left show as follows from top to bottom: Z'-factor, SB (Signal-to-Background) ratio, CV (Coefficient of Variation) for the negative control, and CV for the positive control.

Although the screening precision was not ensured, the compound with significantly higher KLD values was selected as a hit compound (Fig3.2.10).

Fig3.2.10

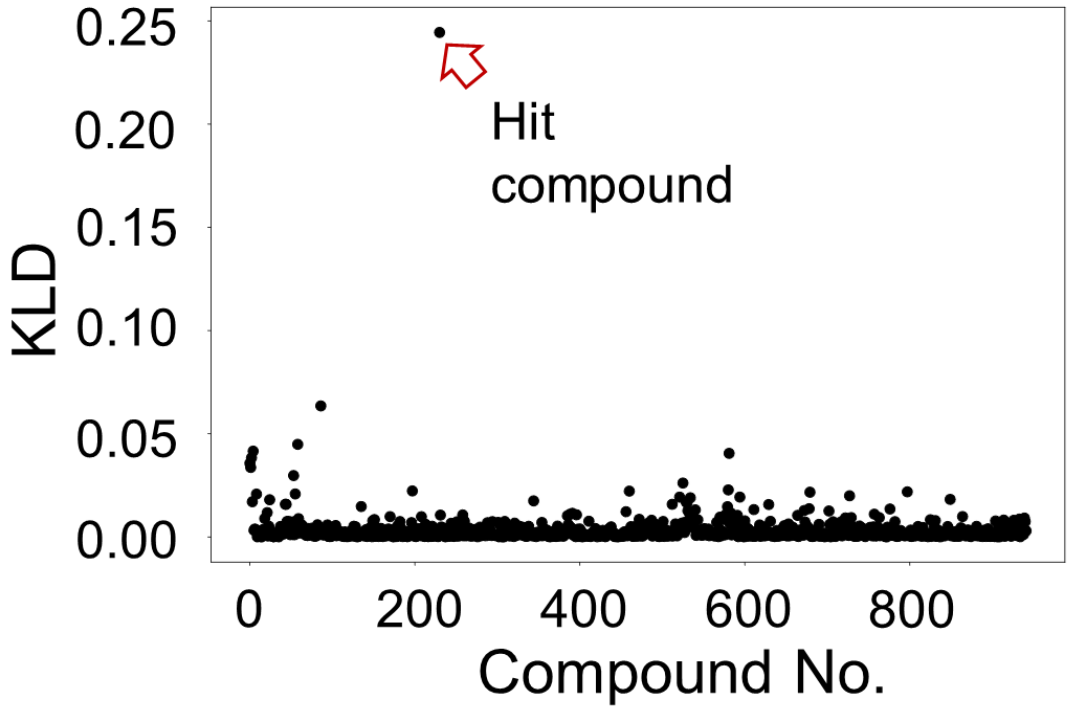

Fig. 3.2.10 Results of drug screening using fluorescence intensity

Result of compound screening based on oligomer formation. The arrow indicates the hit compound (verteporfin).

The compound that significantly altered KLD was verteporfin and revealed a dose-dependent decrease in the fluorescence intensity (Fig3.2.11). Verteporfin is a photosensitizing agent used for the treatment of age-related macular degeneration [42]. Notably, as detailed below, the decrease of fluorescence intensity was turned out not to be caused by its effect on the oligomer formation itself.

Fig3.2.11

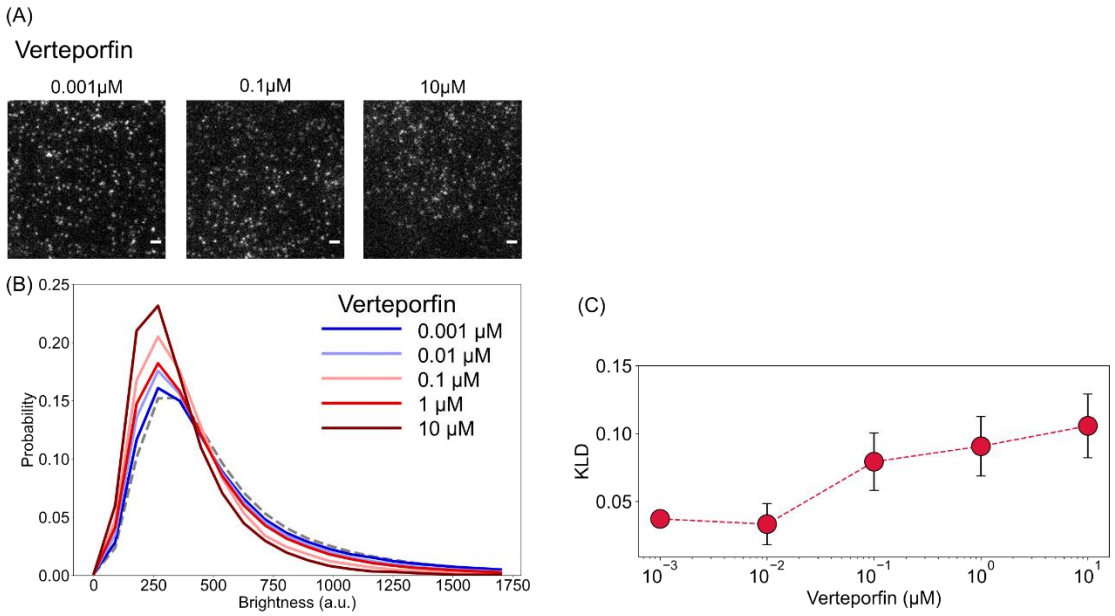

Fig. 3.2.11 Measurement of fluorescence intensity following EGF stimulation

(A) Images obtained from cells treated with verteporfin at concentrations of 0.001 μM, 0.1 μM, and 10 μM. The scale bar is 5 μm. (B) Histograms of fluorescence intensity of bright spot. Higher concentrations of verteporfin resulted in an increase in proportion of monomers. (C)The data represent KLD under conditions without verteporfin stimulation and with verteporfin stimulation at various concentrations. Data represents the mean ± SD from 4 independent experiments.

3.3Characterization of hit compounds on EGFR dynamics, signal transduction, and cell viability

3.3.1 Signal transduction

To investigate whether the selected compounds unrecognized as EGFR inhibitors affect the EGFR signaling, we quantified EGFR phosphorylation, EGFR expression levels, and ERK phosphorylation in CHO- K1 cells expressing EGFR-mEGFP used for the screening. The results showed that none of the compounds inhibited EGFR phosphorylation. However, ERK phosphorylation was affected by Broxyquinoline, Daunorubicin, Eltrombopag, Sorafenib, and Verteporfin. On the other hand, Glafenine and Nilotinib did not reduce ERK phosphorylation (Fig3.3.1).

Fig3.3.1

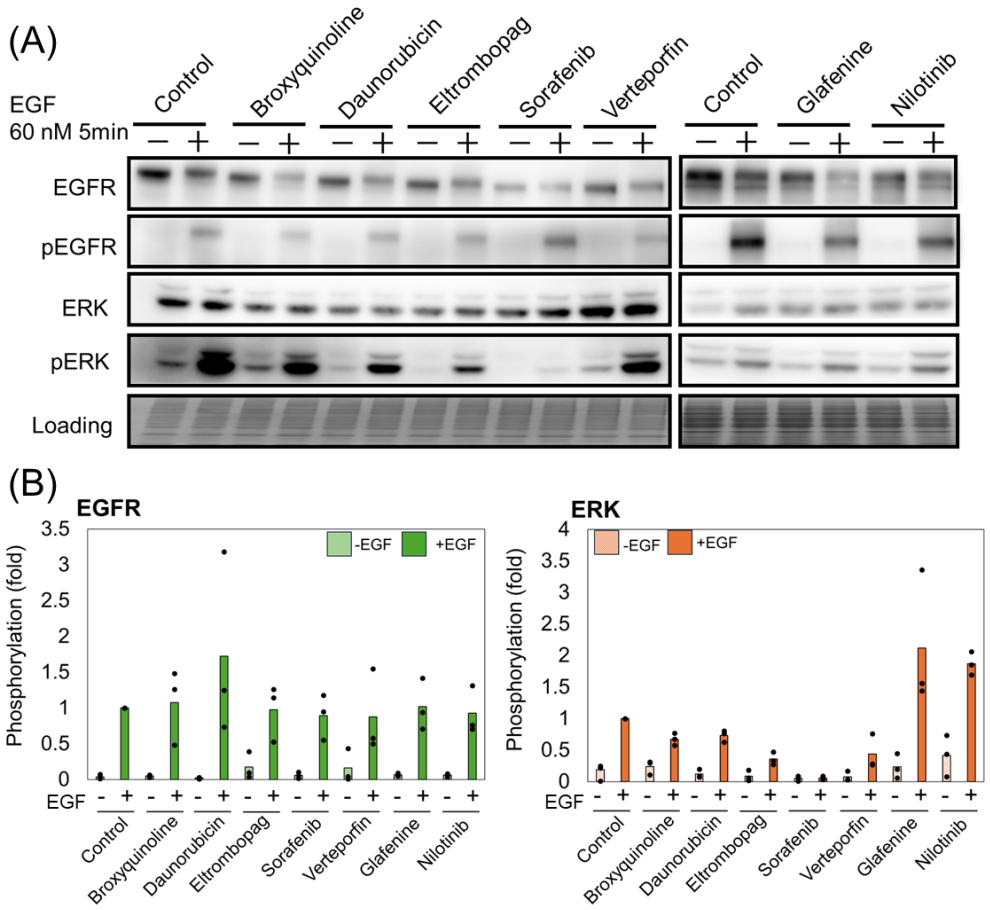

Fig. 3.3.1 Phosphorylation of EGFR and ERK in cells treated with compounds unidentified as EGFR inhibitors

(A) Western blot results showing the phosphorylation of EGFR and ERK before and after EGF stimulation (60 nM for 5 min) in CHO-K1 cells expressing EGFR-mEGFP treated with compounds at 10 μM for 1 hour. (B) Quantification of EGFR and ERK phosphorylation obtained from 3 trials. Dashed boxes represent the average values before EGF addition, while filled boxes denote the average after EGF addition. From 3 independent experiment, each data point corresponds to one trial.

Additionally,, the quantification of total EGFR (expression level) revealed that treatment with the 5 compounds (Broxyquinoline, Daunorubicin, Eltrombopag, Sorafenib, and Verteporfin) decreased EGFR levels, suggesting destabilization of the receptor (Fig3.3.2).

Fig3.3.2

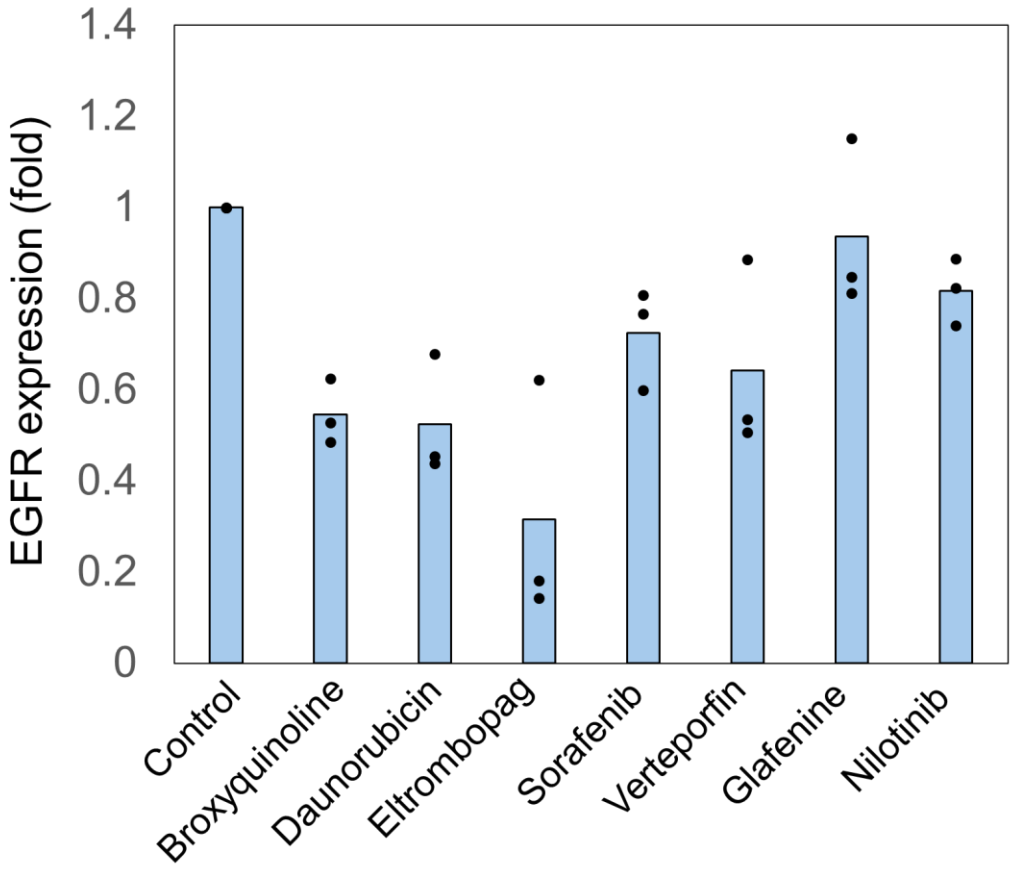

Fig. 3.3.2 Expression levels of EGFR on treatment with unidentified EGFR inhibitor
EGFR expression levels normalized by that of the loading control. This quantification allows for the comparison of EGFR expression before and after compound treatment. From 3 independent experiment, each data point corresponds to one trial.

Furthermore, the total fluorescence intensity of EGFR-mEGFP on the cell membrane was measured for compounds treated cells using single-molecule imaging. The fluorescence intensity did not declined in cells treated by Glafenine and Nilotinib (Fig3.3.3), on the other hand, Broxyquinoline, Daunorubicin, Eltrombopag, Sorafenib, and Verteporfin decrease the intensity over time. In these experiments, Verteporfin causes damage to GFP, therefore, observations were conducted every 20 minutes. These results indicate that Broxyquinoline, Daunorubicin, Eltrombopag, Sorafenib, and Verteporfin could negatively regulate EGFR signaling by promoting EGFR internalization. In other words, drug screening useing single-molecule imaging identified compounds those suppressed EGFR signaling as well as inhibited EGFR tyrosine phosphorylation.

Fig3.3.3

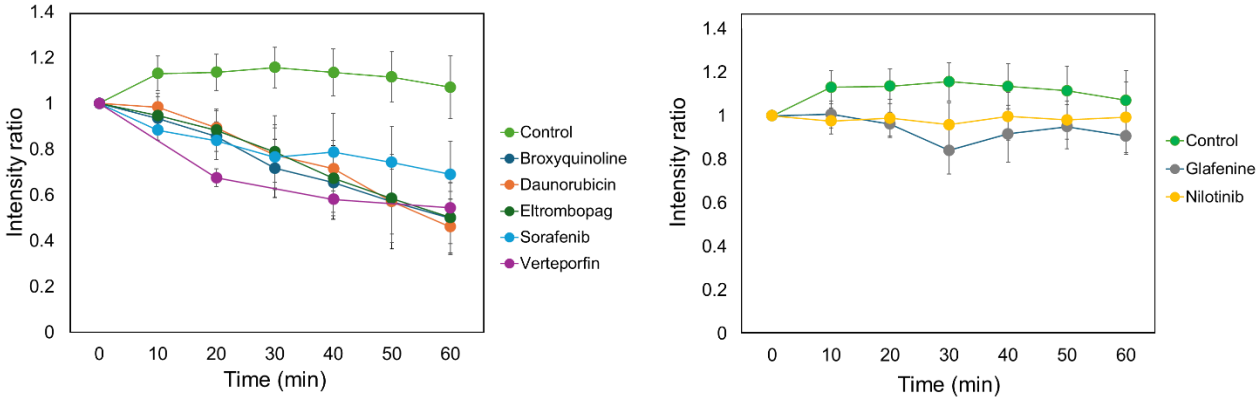

Fig. 3.3.3 Broxyquinoline, Daunorubicin, Eltrombopag, Sorafenib, and Verteporfin reduce EGFR on the cell membrane

Single-molecule imaging was performed at 10-minute intervals on cells expressing EGFR-mEGFP after treatment with compounds (Broxyquinoline, Daunorubicin, Eltrombopag, Sorafenib, Glafenine, Nilotinib). In case of Verteporfin, capturing images at 20-minute intervals. Data are presented as mean ± SD from n = 56, 61, 72, 47, 63, 42, and 46 cells.

3.3.2 Cell viability

To investigate whether the compounds affect the cells, cell viability assays were performed using three cell types expressing EGFR (A431, Hela, and EGFR-transfected Ba/F3) and two cell types not expressing EGFR (CHO-K1 and Ba/F3). Since the former three types of cells are likely to utilize the EGFR signaling pathway for survival, the compounds were considered to act on the viability with an EGFR-dependent manner.

The cell viability assays revealed that EGFR-TKIs, such as Afatinib, Erlotinib, Gefitinib, Lapatinib, Ponatinib, Vandetanib, Dasatinib, and Ibrutinib, reduced the survival rates of A431 and Ba/F3-EGFR cells (Fig3.3.4 left) that is consistent with previous studies about EGFR dependent cell survival [43], [44]. While Hela cells showed resistance to some of these EGFR-TKIs, they exhibited reduced survival rates with Erlotinib and Gefitinib, consistent with the previous reports [45], [46]. In contrast, compounds not targeting EGFR, such as Broxyquinoline, Daunorubicin, Eltrombopag, Sorafenib, and Verteporfin, reduced survival rates in these EGFR-expressing cells, while Glafenine and Nilotinib did not. None of these compounds affected the survival rates of cells without expressing EGFR (Fig3.3.4 right). These findings suggest that Broxyquinoline, Daunorubicin, Eltrombopag, Sorafenib, and Verteporfin suppress EGFR-dependent cell survival and EGFR signaling.

Fig3.3.4

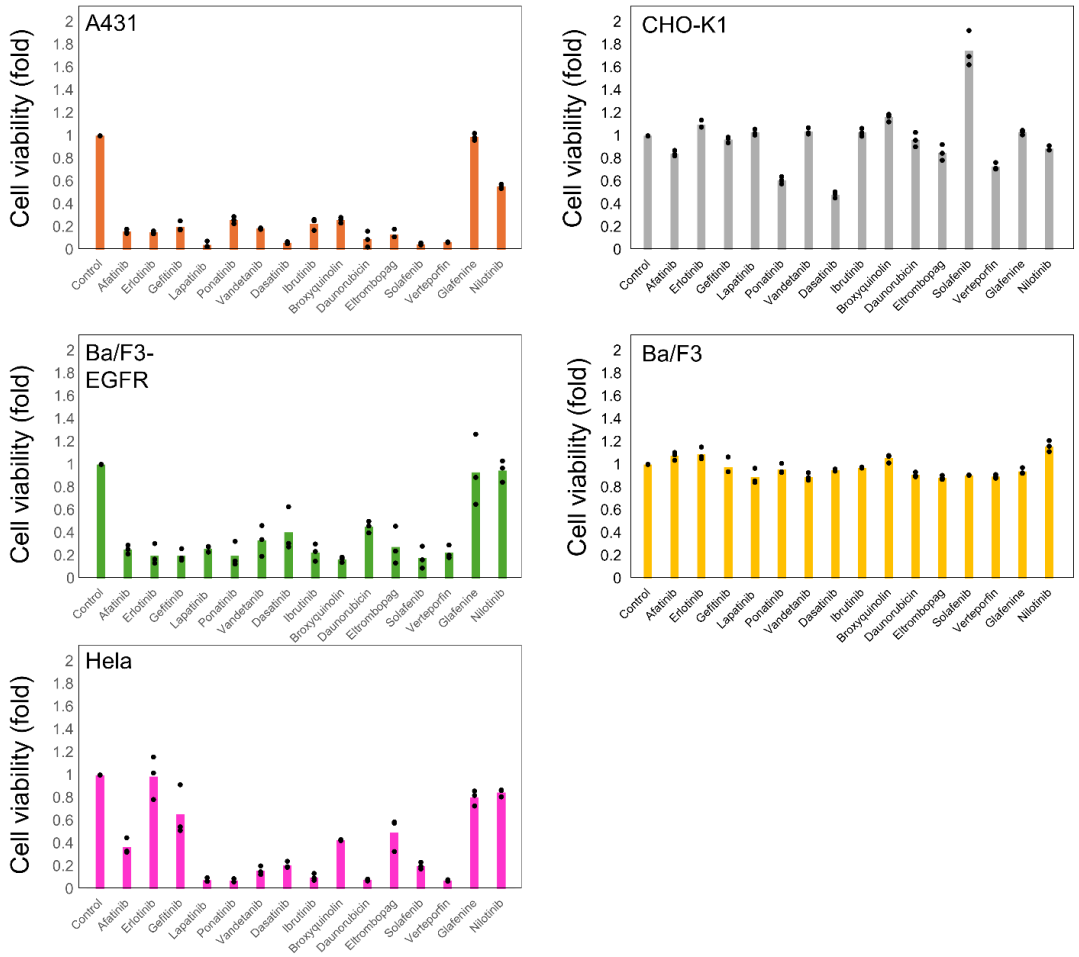

Fig. 3.3.4 Broxyquinoline, Daunorubicin, Eltrombopag, Sorafenib, and Verteporfin reduce EGFR-dependent cell survival

Viability of cells incubated in10 μM EGFR-TKIs and non-TKIs for 72 hours. A431, Ba/F3-EGFR, Hela cells express EGFR. CHO-K1 and Ba/F3 cells do not express EGFR. Bar graphs represent the mean of each trial which is normalized by that in DMSO treated cells. From 3 independent experiment, each data point corresponds to one trial.

3.3.3 Effect of compound on EGFR signaling in various cell types

From the obtained results, it was found that compounds unrecognized as EGFR inhibitors destabilized EGFR and promoted its internalization, that is, inhibition of EGFR-dependent signaling. To further explore the effect of these compounds on other cell types, A431, Ba/F3-EGFR, and Hela were also examined for their EGFR signaling pathways (Fig3.3.5). In the conditions treated with Broxyquinoline, Daunorubicin, Sorafenib, Glafenine, and Nilotinib, EGFR phosphorylation was observed in A431, HeLa, and EGFR-transfected Ba/F3 cells, with rarely difference in the EGFR expression levels. On the other hand, in the conditions treated with Eltrombopag and Verteporfin in EGFR-transfected Ba/F3 cells, the degree of phosphorylation was lower. This is thought to be due to a decrease in the EGFR expression levels themselves

Fig3.3.5

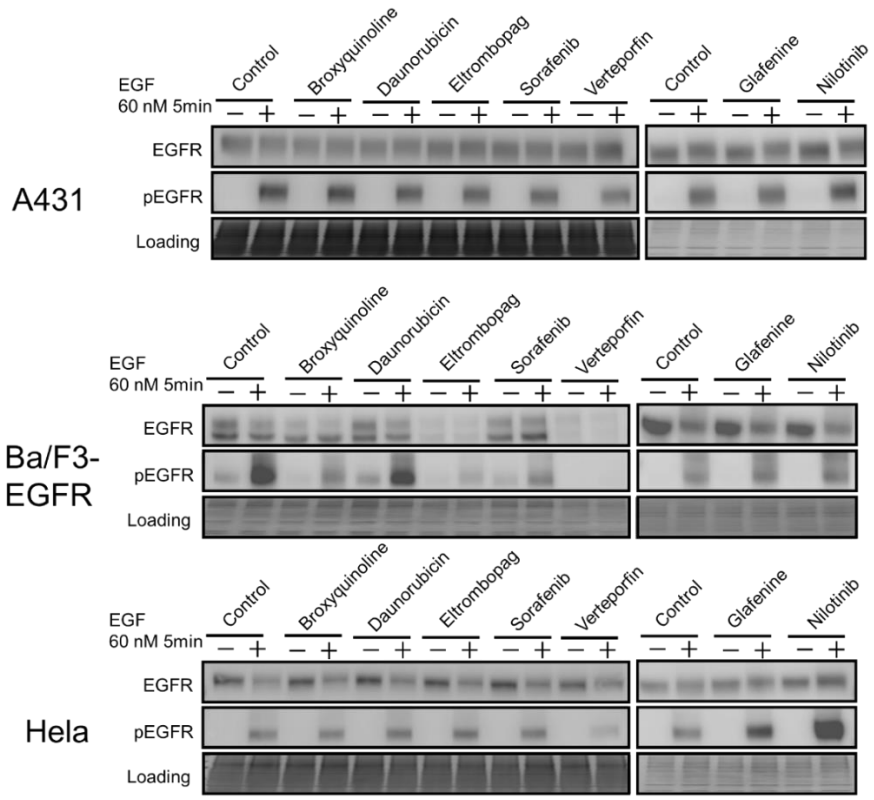

Fig. 3.3.5 Phosphorylation of EGFR in multiple cell types

Western blot analysis was performed on A431, Ba/F3-EGFR, and HeLa cells treated with compounds at 10μM for 1 hour and stimulated with 60 nM EGF for 5 min.

Fig3.3.6

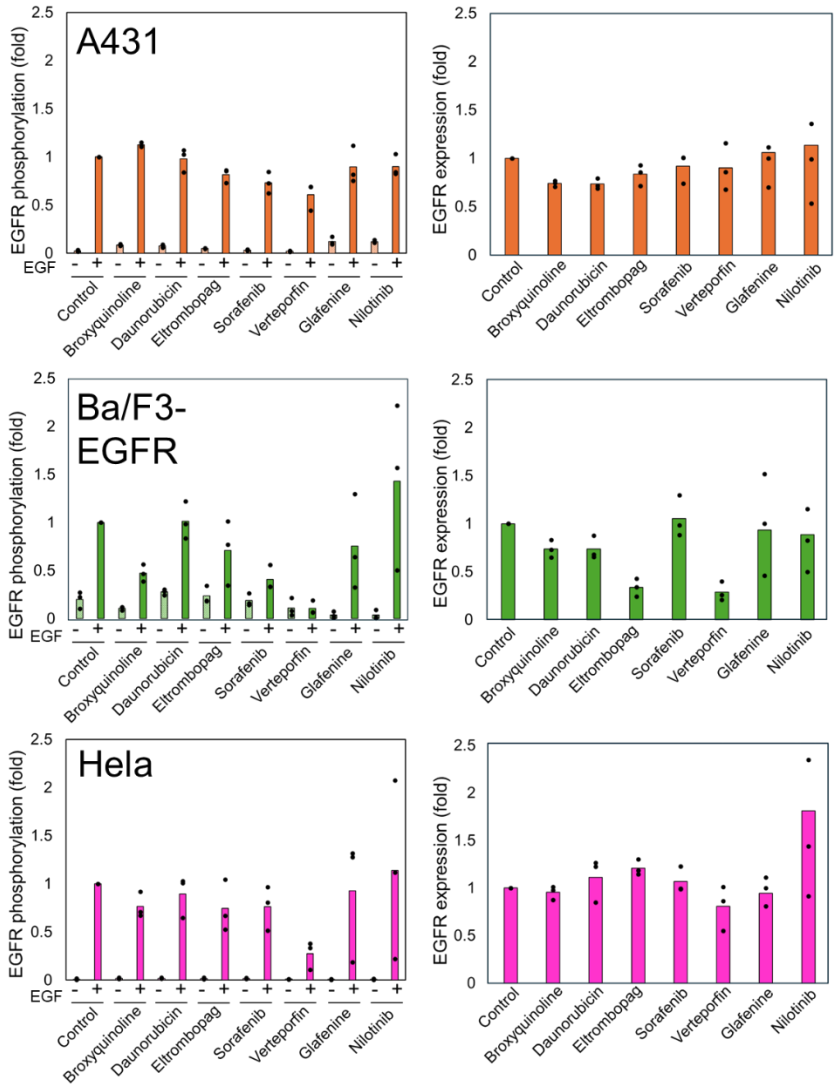

Fig. 3.3.6 Effect of Unidentified EGFR inhibitory compounds on EGFR phosphorylation and expression in A431, Ba/F3-EGFR, and HeLa Cells

Quantification of EGFR phosphorylation and expression levels following treatment with Broxyquinoline, Daunorubicin, Eltrombopag, Sorafenib, Verteporfin, Glafenine, and Nilotinib. The left column shows EGFR phosphorylation with dashed and filled boxes representing averages before and after EGF addition, respectively. The right column shows EGFR expression levels for the compounds-only treatment, which are normalized by that for loading controls. Each black dot represents one experimental trial.

Next, immunofluorescence staining was used to observe EGFR internalization and destabilization. For non-TKIs compound (Broxyquinoline, Daunorubicin, Eltrombopag, Sorafenib, Verteporfin, Glafenine, and Nilotinib) treated A431, Ba/F3-EGFR, and Hela cells (Fig 3.3.6), quantification of fluorescence intensity on the cell membrane was performed. In the case of daunorubicin, it exhibits auto-fluorescence in the nucleus at 488 nm excitation, EGFR was observed using a second antibody with 640 nm excitation. The results showed that treatment with Broxyquinoline, Daunorubicin, Eltrombopag, Sorafenib, and Verteporfin resulted in a decrease in both membrane-bound EGFR and overall cellular fluorescence compared to untreated cells, indicating that these 5 compounds indued EGFR internalization (Fig 3.3.7). In contrast, Glafenine and Nilotinib did not impact on EGFR localization on the membrane (Fig 3.3.7). These experiments revealed that compounds inducing EGFR internalization and degradation could reduce EGFR-dependent signaling and cell viability. Some compounds changing EGFR mobility did not affect the signaling pathways and viability.

Fig3.3.6

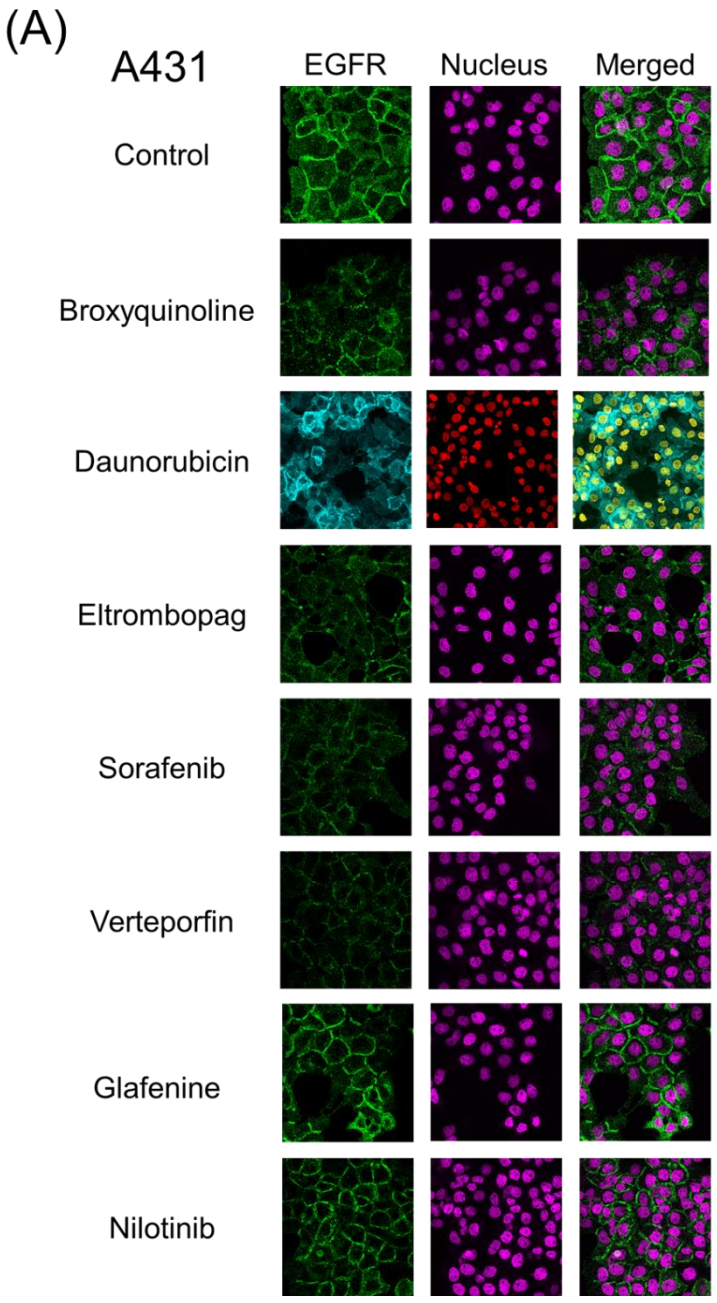
(A)
A431
EGFR
Nucleus
Merged
Control
Broxyquinoline
Daunorubicin
Eltrombopag
Sorafenib
Verteporfin
Glafenine
Nilotinib

Fig3.3.6

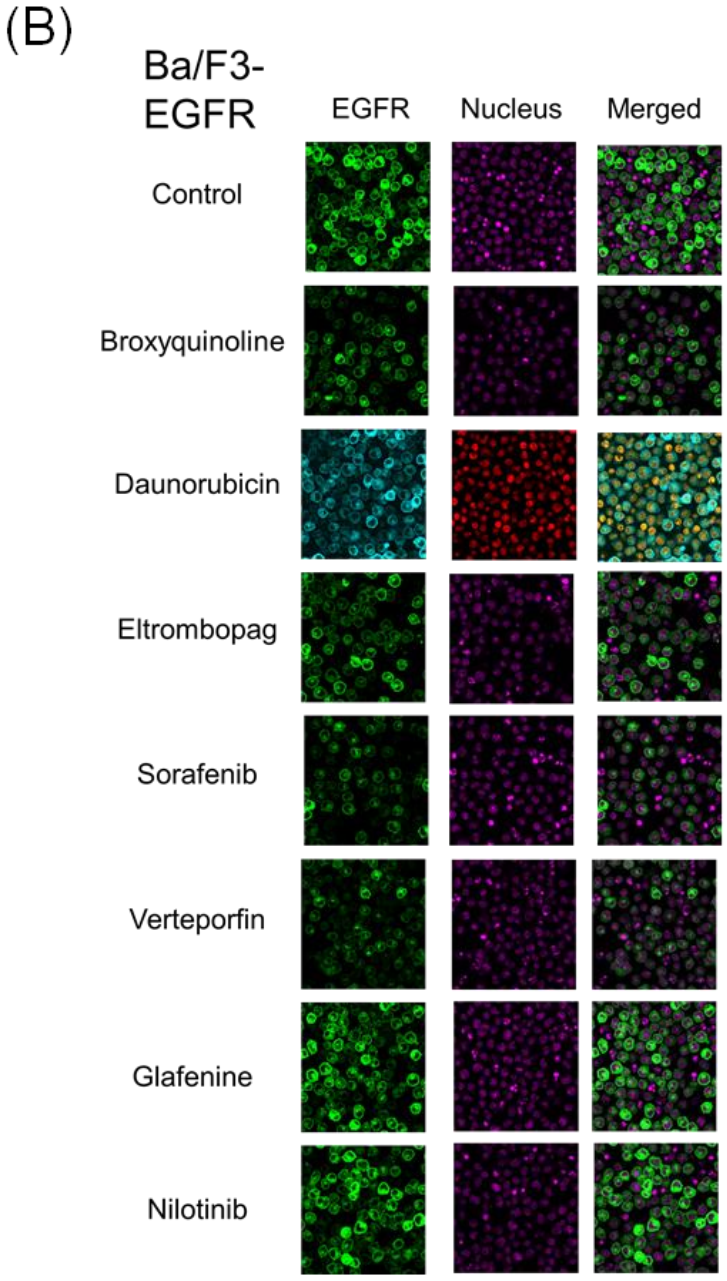
(B)
Ba/F3-EGFR
EGFR
Nucleus
Merged
Control
Broxyquinoline
Daunorubicin
Eltrombopag
Sorafenib
Verteporfin
Glafenine
Nilotinib

Fig3.3.6

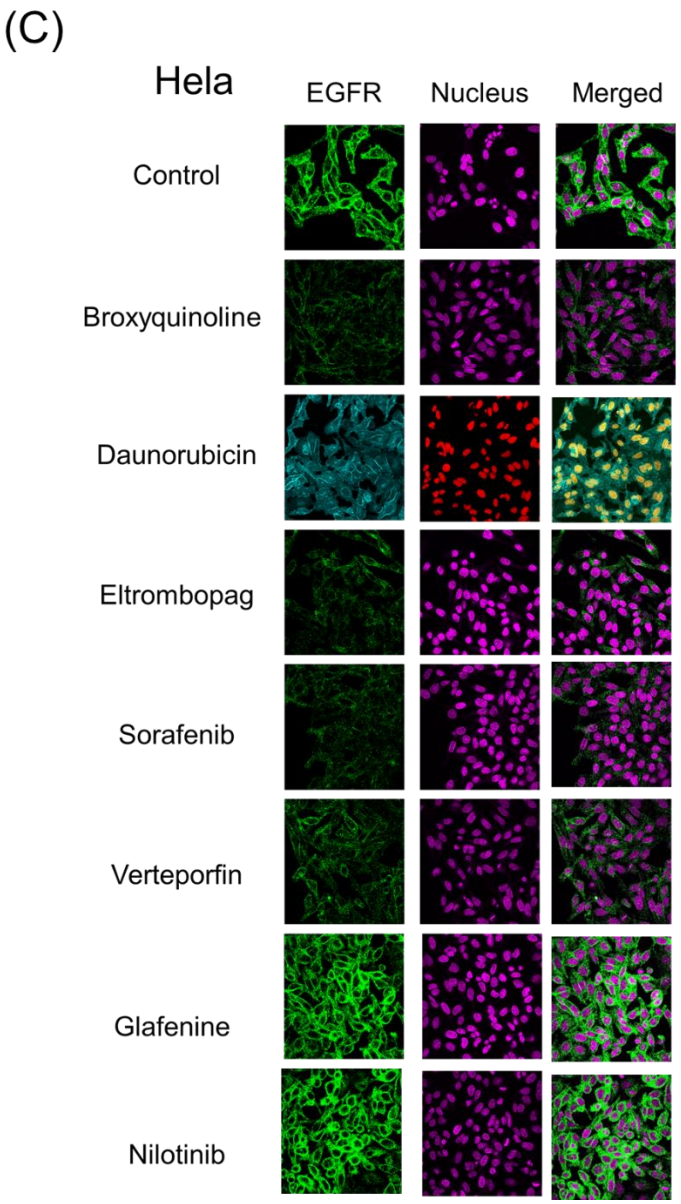

Fig. 3.3.6 immunofluorescence assay for A431, Ba/F3-EGFR, Hela cells after the compound treatment

After compound treatment for 1 hour at 10μM in A431, Ba/F3-EGFR, and HeLa cells, fluorescence immunostaining was performed. Due to the fluorescent properties of daunorubicin, EGFR was visualized at 640 nm, while other compounds were visualized at 488 nm. Nuclei were stained to identify and distinguish cells. (A) A431 cells, (B) Ba/F3-EGFR cells, and (C) HeLa cells.

Fig3.3.7

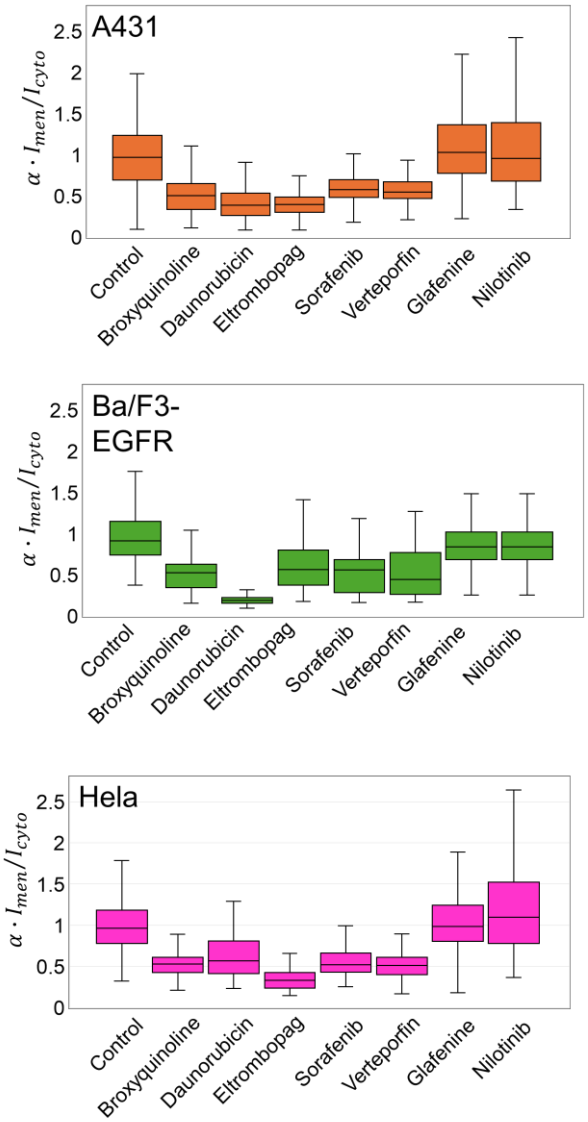

Fig. 3.3.7 Broxyquinoline, Daunorubicin, Eltrombopag, Sorafenib, and Verteporfin Induce EGFR Internalization and Degradation

Internalization and degradation were calculated using cell membrane and intracellular fluorescence intensities, represented as $\alpha \cdot I_{mem}/ I_{cyt}$. Box-and-whisker plots illustrate the median as horizontal lines, first and third quartiles as box ends. Data were collected from 332, 326, 177, 402, 476, 282, and 454 A431 cells; 562, 406, 322, 422, 446, 564, and 506 Ba/F3 cells expressing EGFR; and 466, 321, 220, 353, 302, 363, 643, and 496 HeLa cells.

3.3.4 Broxyquinoline related to caveolin induced internalization

Compounds obtained by single-molecule tracking-based drug screening, Broxyquinoline, Daunorubicin, Eltrombopag, Sorafenib, and Verteporfin were found to play a role in the internalization of EGFR. These compounds inhibiting EGFR mobility may cause aggregation in specific regions. Broxyquinoline is known to increase the expression of hypoxia-inducible factors (HIF), which is involved in the accumulation of caveolin [47], [48], [49]. To verify the similar process occurs in CHO-K1 cells treated with Broxyquinoline, the accumulation of HIF1 and caveolin in these cells was observed (Fig. 3.8.8A). The results showed an increase in HIF1 following Broxyquinoline treatment. Although no significant increase in caveolin expression was observed, its internalization was confirmed (Fig. 3.8.8B). These results demonstrate an increase in HIF1α expression following Broxyquinoline treatment, along with internalization of caveolin, indicating its role in the internalization of EGFR.

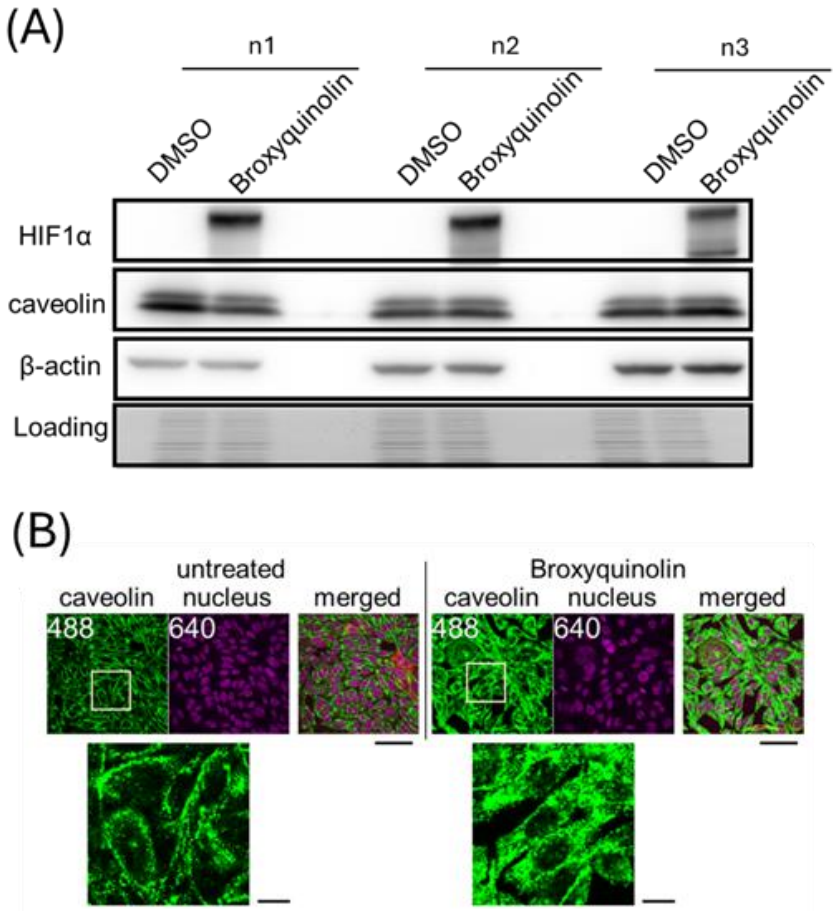

Figure 3.3.8: HIF1α expression and EGFR internalization with caveolin

(A) In CHOK1-EGFR cells treated with 10 µM Broxyquinoline for 1 hour, Western blot analysis was performed to observe the expression of HIF1α and caveolin. Data are representative of 3 independent experiments. **(B)** Under the same treatment conditions, immunofluorescence staining was carried out to visualize caveolin. Scale bar represents 100 µm. Caveolin and nuclei were stained with Alexa 488 and NucSpot Live 650 with excitation by lasers at 488 nm and 650 nm.

Chapter 4

Discussion

4.1 Validation of drug screening using single-molecule imaging

In this study, I evaluated the utility of the single-molecule tracking-based drug screening by focusing on the mobility and clustering of EGFR molecules. By performing this screening on the library of 1,134 FDA-approved drugs including EGFR inhibitors all EGFR inhibitors that suppressed the EGF-induced decrease in EGFR mobility were successfully detected. After binding to the ligand, EGFR is known to relocate to specific regions, such as lipid rafts [18], [23], with reduction of the mobility during the dimerization and multimerization process followed by autophosphorylation. The binding of EGFR TKIs to the ATP-binding pocket prevents from EGFR phosphorylation, inhibiting its relocation to confined regions. The changes in mobility could be detected sensitively by single-molecule screening, therefore, all EGFR TKIs in the library were selected. Single-molecule imaging is shown to be an effective approach to screen EGFR TKIs.

4.2 Single-molecule tracking-based drug screening detect non-EGFR TKI

By the single-molecule tracking based drug screening, compounds not previously recognized as EGFR TKIs but affecting EGFR-dependent signaling and cell responses were obtained. These compounds included Broxyquinoline, Daunorubicin, Eltrombopag, Sorafenib, Verteporfin, Glafenine, and Nilotinib. These compounds were found to affect the EGFR signaling pathway by internalizing EGFR molecules on the cell membrane. Interestingly, these compounds caused a reduction in the EGFR mobility, suggesting relocating to specific subdomains of the cell membrane. For example, treatment with Broxyquinoline resulted in the accumulation of caveolin, a protein associated with hypoxia-induced factor (HIF-1) expression, indicating a mechanism of EGFR internalization through changes in membrane environment around EGFR molecules. This internalization could contribute to the inhibition of EGFR signaling, causing the decrease in cell viability.

On the other hand, compounds such as Glafenine and Nilotinib altered EGFR mobility but not affecting both EGFR internalization and cell viability. The mechanism reducing the EGFR mobility remains unclear, but these compounds might affect another signaling or cellular event except those assessed in the current study.

The findings suggest that single-molecule tracking-based drug screening is capable of detecting not only compounds that directly influence EGFR phosphorylation but also compounds that could not be identified through conventional phosphorylation-based screening. However, determining whether these compounds directly affect EGFR signaling requires integration with complementary assays.

4.3 Improving throughput of single-molecule imaging screening for practical drug discovery applications

Single-molecule tracking-based drug screening enables the detection of compounds targeting multiple processes involved in signaling pathways by measuring mobility and clustering. This method requires only conjugating of proteins with fluorescent probes, making it broadly applicable to various membrane proteins beyond the EGFR. It has previously been known that lateral diffusion of various receptors changed upon activation, such as GPCRs and nuclear receptors other than EGFR [50], [51], [52]. It is preferable to enhance the throughput of this technique comparable to high-throughput screening (HTS). In the current setup, data acquisition for 1 compound takes approximately 2 minutes to capture images from 40 cells (Fig 3.2.1C). Compared to traditional single-molecule imaging, efficiency is improved 50-fold. However, it remains significantly slower than typical methods of HTS such as absorbance measurement using plate readers, which processes 1 compound in about 0.5 seconds and approximately 240 times faster than single-molecule imaging. The primary bottleneck process in single-molecule imaging is the cell searching, which takes approximately 75 seconds. The image acquisition process for 40 cells adds further time.

Adopting technologies such as wide-field TIRF illumination, which is currently under development, could resolve this bottleneck. By illuminating the entire well with total internal reflection, it would be possible to execute image acquisition in which each image contains more than 40 cells. It eliminates the cell searching process, reducing the required time by 75 seconds per well. These advancements would significantly expand the utility of single-molecule imaging in membrane protein-targeted drug discovery.

4.4 Appendix (data for screened compounds)

#	Name	Target	Relative MSD ratio (fold)
1	Phenoxybenzamine	Membrane receptors	0.75
2	Pramipexole	Membrane receptors	0.6
3	Formoterol	Membrane receptors	0.63
4	Mirtazapine	Membrane receptors	0.83
5	Fesoterodine	Membrane receptors	0.81
6	Ritodrine	Membrane receptors	0.72
7	Conivaptan	Membrane receptors	0.71
8	Dronedarone	Membrane receptors	0.86
9	Dopamine	Membrane receptors	0.87
10	Clemastine	Membrane receptors	0.86
11	Xylazine	Membrane receptors	0.88
12	Valsartan	Membrane receptors	0.7
13	Erlotinib	Membrane receptors	3.86
14	Epinephrine Bitartrate	Membrane receptors	0.91
15	Atropine	Membrane receptors	0.79
16	Ketotifen Fumarate	Membrane receptors	0.82
17	Diphenhydramine	Membrane receptors	0.41
18	Adrenaline	Membrane receptors	0.91
19	Naftopidil	Membrane receptors	0.73
20	Metoprolol	Membrane receptors	0.55
21	Sotalol	Membrane receptors	0.79
22	Nizatidine	Membrane receptors	0.82
23	Aspartame	Membrane receptors	0.87
24	Maraviroc	Membrane receptors	0.79
25	Salbutamol	Membrane receptors	0.75
26	Candesartan	Membrane receptors	ND
27	Adrenaline	Membrane receptors	0.74
28	Phentolamine	Membrane receptors	0.82
29	Naphazoline	Membrane receptors	0.83
30	Urapidil	Membrane receptors	0.91
31	Scopolamine	Membrane receptors	0.89
32	Levobetaxolol	Membrane receptors	1.01
33	Tiotropium	Membrane receptors	1.08
34	Misoprostol	Membrane receptors	1.12
35	Metaproterenol Sulfate	Membrane receptors	0.92
36	Mesoridazine	Membrane receptors	0.66
37	Isoetharine	Membrane receptors	0.45
38	Prochlorperazine	Membrane receptors	0.84
39	Pindolol	Membrane receptors	0.74
40	Diphenylpyraline	Membrane receptors	0.85
41	Lofexidine	Membrane receptors	0.9
42	Eltrombopag	Membrane receptors	1.8
43	Citrate	Membrane receptors	0.7
44	Anisotropine	Membrane receptors	0.8
45	Pimozide	Membrane receptors	0.88
46	Azelastine	Membrane receptors	0.87
47	Pyrilamine	Membrane receptors	0.85
48	Serotonin	Membrane receptors	0.8
49	Doxylamine	Membrane receptors	0.83
50	Pipenzolate	Membrane receptors	0.85

51	Pilocarpine	Membrane receptors	0.87
52	Bromocriptine	Membrane receptors	0.91
53	Plerixafor	Membrane receptors	0.9
54	Methoxamine	Membrane receptors	0.98
55	Nalmefene	Membrane receptors	0.9
56	Otilonium	Membrane receptors	1.27
57	Aceclidine	Membrane receptors	1.04
58	Mepenzolate	Membrane receptors	0.97
59	Thioridazine	Membrane receptors	0.87
60	Dicyclomine	Membrane receptors	1.01
61	Triflupromazine	Membrane receptors	0.92
62	Metaraminol	Membrane receptors	0.86
63	Pheniramine	Membrane receptors	1.03
64	Tolvaptan	Membrane receptors	1.06
65	Moxonidine	Membrane receptors	1.32
66	Carbachol	Membrane receptors	0.99
67	Bismuth	Membrane receptors	0.93
68	Benztropine	Membrane receptors	0.92
69	Terfenadine	Membrane receptors	1.08
70	Ractopamine	Membrane receptors	1.06
71	Apomorphine	Membrane receptors	1.21
72	Procyclidine	Membrane receptors	1.07
73	Almotriptan	Membrane receptors	0.85
74	Oxprenolol	Membrane receptors	0.95
75	Hyoscyamine	Membrane receptors	0.98
76	Desloratadine	Membrane receptors	0.65
77	Acebutolol	Membrane receptors	0.91
78	Mirabegron	Membrane receptors	0.79
79	Rimonabant	Membrane receptors	1.06
80	Cimetidine	Membrane receptors	0.67
81	Betahistine	Membrane receptors	0.88
82	Pazopanib	Membrane receptors	1.06
83	Ticagrelor	Membrane receptors	1.71
84	Propranolol	Membrane receptors	0.81
85	Ipratropium	Membrane receptors	0.94
86	Guanabenz Acetate	Membrane receptors	0.9
87	Noradrenaline	Membrane receptors	0.6
88	Tripelennamine	Membrane receptors	1.1
89	Choline Chloride	Membrane receptors	1
90	Darifenacin	Membrane receptors	1
91	Doxofylline	Membrane receptors	1.25
92	Orphenadrine	Membrane receptors	1
93	Haloperidol	Membrane receptors	0.94
94	Tropicamide	Membrane receptors	1.11
95	Tolterodine	Membrane receptors	0.95
96	Trospium	Membrane receptors	0.96
97	Alfuzosin	Membrane receptors	1.31
98	Loxapine Succinate	Membrane receptors	1.03
99	Cyproheptadine	Membrane receptors	0.9
100	Bismuth	Membrane receptors	1.05
101	Azatadine	Membrane receptors	1.25

102	Medetomidine	Membrane receptors	1.12
103	Histamine	Membrane receptors	0.94
104	Azilsartan	Membrane receptors	0.91
105	Solifenacin	Membrane receptors	1.05
106	Pergolide	Membrane receptors	1.15
107	Montelukast	Membrane receptors	1.23
108	Fexofenadine	Membrane receptors	1.03
109	Meptazinol	Membrane receptors	0.97
110	Azilsartan	Membrane receptors	1.07
111	Lurasidone	Membrane receptors	0.86
112	Eprosartan	Membrane receptors	1.14
113	Droxidopa	Membrane receptors	1.29
114	Esmolol	Membrane receptors	1.01
115	Fosaprepitant	Membrane receptors	0.86
116	Bepotastine	Membrane receptors	1.12
117	Droperidol	Membrane receptors	1.19
118	Trifluoperazine	Membrane receptors	0.86
119	Ropinirole	Membrane receptors	0.93
120	Antazoline	Membrane receptors	0.9
121	Adrenalone	Membrane receptors	0.91
122	Blonanserin	Membrane receptors	0.6
123	Afatinib	Membrane receptors	2.63
124	Lapatinib	Membrane receptors	3.8
125	Oxybutynin	Membrane receptors	0.87
126	Imatinib	Membrane receptors	1.21
127	Aminophylline	Membrane receptors	1.01
128	Famotidine	Membrane receptors	0.91
129	Losartan	Membrane receptors	0.98
130	Ramelteon	Membrane receptors	0.86
131	Biperiden	Membrane receptors	0.93
132	Loperamide	Membrane receptors	1.03
133	Methyldopa	Membrane receptors	0.67
134	Gallamine	Membrane receptors	0.93
135	Cinacalcet	Membrane receptors	0.54
136	Asenapine	Membrane receptors	0.91
137	Aripiprazole	Membrane receptors	1.06
138	Ambrisentan	Membrane receptors	1.03
139	Naratriptan	Membrane receptors	1.09
140	Cetirizine	Membrane receptors	1.12
141	Zolmitriptan	Membrane receptors	0.79
142	Pranlukast	Membrane receptors	1.37
143	Nebivolol	Membrane receptors	1.02
144	Carvedilol	Membrane receptors	1.25
145	Meglumine	Membrane receptors	0.95
146	Bethanechol	Membrane receptors	0.76
147	Prasugrel	Membrane receptors	1.12
148	Chlorpromazine	Membrane receptors	0.69
149	Pramipexole	Membrane receptors	0.88
150	Masitinib	Membrane receptors	1.07
151	Iloperidone	Membrane receptors	0.85
152	Vandetanib	Membrane receptors	1.67

153	Ranitidine	Membrane receptors	0.63
154	Crizotinib	Membrane receptors	1.08
155	Clozapine	Membrane receptors	0.71
156	Vismodegib	Membrane receptors	0.55
157	Sunitinib	Membrane receptors	ND
158	Cabozantinib	Membrane receptors	1.22
159	Bimatoprost	Membrane receptors	1
160	Acetylcholine	Membrane receptors	0.76
161	Clonidine	Membrane receptors	0.65
162	Trimebutine	Membrane receptors	0.89
163	Axitinib	Membrane receptors	1.16
164	Cilostazol	Membrane receptors	0.96
165	Dexmedetomidine	Membrane receptors	1.03
166	Betaxolol	Membrane receptors	0.85
167	Chlorpheniramine	Membrane receptors	0.79
168	Detomidine	Membrane receptors	0.97
169	Aprepitant	Membrane receptors	1.03
170	Naltrexone	Membrane receptors	1.03
171	Levosulpiride	Membrane receptors	0.97
172	Betaxolol hydrochloride	Membrane receptors	1.1
173	Prazosin	Membrane receptors	1.38
174	Lapatinib	Membrane receptors	2.67
175	Imatinib Mesylate	Membrane receptors	0.99
176	Adenine	Membrane receptors	1.06
177	Quetiapine	Membrane receptors	0.91
178	Ziprasidone	Membrane receptors	1.03
179	Gefitinib	Membrane receptors	2.82
180	Ticlopidine	Membrane receptors	1.01
181	Erlotinib	Membrane receptors	2.44
182	Olanzapine	Membrane receptors	1.07
183	Adenine	Membrane receptors	1.14
184	Olopatadine	Membrane receptors	0.65
185	Dasatinib	Membrane receptors	2.4
186	Zafirlukast	Membrane receptors	0.85
187	Doxazosin	Membrane receptors	1.29
188	Sumatriptan	Membrane receptors	0.96
189	Meclizine	Membrane receptors	0.67
190	Agomelatine	Membrane receptors	0.96
191	Oxymetazoline	Membrane receptors	0.8
192	Chlorprothixene	Membrane receptors	0.96
193	Alprostadil	Membrane receptors	0.84
194	Irbesartan	Membrane receptors	0.82
195	Adenine	Membrane receptors	1.08
196	Domperidone	Membrane receptors	0.97
197	Mizolastine	Membrane receptors	1.05
198	Dyphylline	Membrane receptors	0.95
199	Pazopanib	Membrane receptors	1.02
200	Amisulpride	Membrane receptors	0.98
201	Amiodarone	Membrane receptors	1.31
202	Tizanidine	Membrane receptors	0.98
203	Clopidogrel	Membrane receptors	0.81

204	Rocuronium	Membrane receptors	0.87
205	Methscopolamine	Membrane receptors	0.86
206	Nilotinib	Membrane receptors	1.86
207	Adenosine	Membrane receptors	0.89
208	Lonidamine	Enzymes	1.42
209	Uridine	Enzymes	0.59
210	Methimazole	Enzymes	0.81
211	Diclofenac	Enzymes	0.97
212	Ibandronate	Enzymes	0.93
213	Ketorolac	Enzymes	0.7
214	Acarbose	Enzymes	0.7
215	Ketoprofen	Enzymes	0.64
216	Uracil	Enzymes	0.84
217	Celecoxib	Enzymes	0.78
218	Moclobemide	Enzymes	1.03
219	Ibuprofen	Enzymes	1.02
220	Carfilzomib	Enzymes	0.94
221	Cobicistat	Enzymes	0.76
222	Diclofenac	Enzymes	0.8
223	Etodolac	Enzymes	0.88
224	Ampiroxicam	Enzymes	0.94
225	Rosuvastatin	Enzymes	1.03
226	Dichlorphenamide	Enzymes	1.14
227	Rasagiline	Enzymes	1.43
228	Benzydamine	Enzymes	1.01
229	Anisindione	Enzymes	0.85
230	Perindopril	Enzymes	0.85
231	Gemcitabine	Enzymes	0.93
232	Sulindac	Enzymes	0.9
233	Temocapril	Enzymes	0.99
234	Sildenafil	Enzymes	0.76
235	Capecitabine	Enzymes	1
236	Tenoxicam	Enzymes	0.77
237	Sodium salicylate	Enzymes	1.01
238	Tadalafil	Enzymes	0.92
239	Rolipram	Enzymes	0.83
240	Cyclosporine	Enzymes	0.86
241	Vardenafil	Enzymes	0.92
242	Oxaprozin	Enzymes	1
243	Methylthiouracil	Enzymes	1.03
244	Mitoxantrone	Enzymes	0.9
245	Risedronate	Enzymes	0.84
246	Rofecoxib	Enzymes	1.14
247	Roflumilast	Enzymes	0.45
248	Leflunomide	Enzymes	0.92
249	Allopurinol	Enzymes	0.92
250	Zaltoprofen	Enzymes	0.82
251	Irinotecan	Enzymes	0.87
252	Dipyridamole	Enzymes	ND
253	Linagliptin	Enzymes	0.89
254	Topotecan	Enzymes	0.97

255	Orlistat	Enzymes	0.84
256	Fenoprofen	Enzymes	0.97
257	Ibuprofen	Enzymes	1
258	Nepafenac	Enzymes	1
259	Bufexamac	Enzymes	0.86
260	Rivastigmine	Enzymes	0.85
261	Pitavastatin	Enzymes	1.19
262	Hydroxyurea	Enzymes	0.88
263	Anagrelide	Enzymes	1.1
264	Esomeprazole	Enzymes	1.02
265	Carbidopa	Enzymes	0.84
266	Fosinopril	Enzymes	0.81
267	Triflusal	Enzymes	0.88
268	Finasteride	Enzymes	1.22
269	Pimobendan	Enzymes	1.55
270	Irinotecan	Enzymes	0.91
271	Cladribine	Enzymes	0.99
272	Voglibose	Enzymes	0.94
273	Dabigatran	Enzymes	0.82
274	Rivaroxaban	Enzymes	0.89
275	Aliskiren	Enzymes	0.73
276	TAME	Enzymes	0.92
277	Dexlansoprazole	Enzymes	1.09
278	Alendronate	Enzymes	0.93
279	Pranoprofen	Enzymes	0.8
280	Pravastatin	Enzymes	0.95
281	Mefenamic	Enzymes	0.65
282	Naproxen	Enzymes	0.95
283	Daunorubicin	Enzymes	1.99
284	Tolfenamic	Enzymes	0.77
285	Exemestane	Enzymes	1
286	Tranexamic	Enzymes	0.81
287	Gabexate	Enzymes	0.9
288	Mofetil	Enzymes	0.84
289	Aspirin	Enzymes	1.01
290	Benazepril	Enzymes	0.86
291	Phenylbutazone	Enzymes	0.66
292	Imidapril	Enzymes	0.93
293	Cytidine	Enzymes	1.05
294	Enalaprilat	Enzymes	0.91
295	Tacrine	Enzymes	1
296	Simvastatin	Enzymes	0.98
297	Racecadotril	Enzymes	0.7
298	Atorvastatin	Enzymes	1.14
299	Carmofur	Enzymes	0.99
300	Lisinopril	Enzymes	0.82
301	Phenindione	Enzymes	1.13
302	Neostigmine	Enzymes	0.83
303	Avanafil	Enzymes	1.05
304	Pemetrexed	Enzymes	1.06
305	Nimesulide	Enzymes	0.76

306	Ramipril	Enzymes	0.71
307	Physostigmine	Enzymes	0.91
308	Moexipril	Enzymes	0.74
309	Captopril	Enzymes	0.86
310	Bortezomib	Enzymes	1.41
311	Glycyrrhizinate	Enzymes	0.88
312	Dabigatran	Enzymes	1.24
313	Cilazapril	Enzymes	0.93
314	Enalapril	Enzymes	0.65
315	Fluvastatin	Enzymes	1.16
316	Propylthiouracil	Enzymes	0.62
317	Zileuton	Enzymes	0.97
318	Ozagrel	Enzymes	0.64
319	Abiraterone	Enzymes	0.89
320	Doxifluridine	Enzymes	0.91
321	Lornoxicam	Enzymes	0.93
322	Donepezil	Enzymes	0.75
323	Esomeprazole	Enzymes	0.83
324	Carbenoxolone	Enzymes	0.92
325	Tolmetin	Enzymes	1
326	Physostigmine	Enzymes	0.88
327	Amfenac	Enzymes	0.95
328	Benserazide	Enzymes	0.91
329	Teniposide	Enzymes	0.83
330	Floxuridine	Enzymes	0.74
331	Valdecoxib	Enzymes	1.01
332	Nabumetone	Enzymes	1.04
333	Aminocaproic	Enzymes	0.91
334	Tegafur	Enzymes	0.77
335	Aminoglutethimide	Enzymes	1.06
336	Ethoxzolamide	Enzymes	0.8
337	Diclofenac	Enzymes	0.75
338	Thioguanine	Enzymes	0.82
339	Risedronic	Enzymes	0.84
340	Mercaptopurine	Enzymes	0.66
341	Acemetacin	Enzymes	1.02
342	Pamidronate	Enzymes	0.94
343	Flurbiprofen	Enzymes	1.02
344	Disulfiram	Enzymes	0.61
345	Zoledronic	Enzymes	0.87
346	Epalrestat	Enzymes	1.12
347	Abiraterone	Enzymes	0.67
348	Rolipram	Enzymes	0.93
349	Carbimazole	Enzymes	1
350	Brinzolamide	Enzymes	0.92
351	Ozagrel	Enzymes	0.83
352	Vorinostat	Enzymes	1.01
353	Thiouracil	Enzymes	0.85
354	Argatroban	Enzymes	0.93
355	Pimecrolimus	Enzymes	0.78
356	Gimeracil	Enzymes	1.06

357	Fludarabine	Enzymes	0.79
358	Mycophenolic	Enzymes	0.96
359	Tacrolimus	Enzymes	0.88
360	Pralatrexate	Enzymes	0.82
361	Azacitidine	Enzymes	0.79
362	Nialamide	Enzymes	0.98
363	Benzoic	Ion channels	1.03
364	Amantadine	Ion channels	0.94
365	Triamterene	Ion channels	0.8
366	Vecuronium	Ion channels	0.98
367	Amlodipine	Ion channels	0.92
368	Nifedipine	Ion channels	0.74
369	Memantine	Ion channels	0.83
370	Rufinamide	Ion channels	0.99
371	Articaine	Ion channels	0.81
372	Flunarizine	Ion channels	0.91
373	Gluconate	Ion channels	0.88
374	Clevidipine	Ion channels	0.75
375	Hexamethonium	Ion channels	0.82
376	Nicardipine	Ion channels	1.08
377	Phenytoin	Ion channels	0.9
378	Tropisetron	Ion channels	0.77
379	Ivabradine	Ion channels	0.85
380	Mepivacaine	Ion channels	0.91
381	Gabapentin	Ion channels	0.99
382	Niflumic	Ion channels	0.72
383	Oxybuprocaine	Ion channels	0.94
384	Valproic	Ion channels	1.03
385	Proparacaine	Ion channels	1.01
386	Topiramate	Ion channels	0.81
387	Atracurium	Ion channels	0.96
388	Disopyramide	Ion channels	0.72
389	Quipazine	Ion channels	0.81
390	Azasetron	Ion channels	0.84
391	Cilnidipine	Ion channels	0.91
392	Diltiazem	Ion channels	0.62
393	Oxethazaine	Ion channels	0.95
394	Nitrendipine	Ion channels	1.27
395	Isradipine	Ion channels	0.89
396	Dofetilide	Ion channels	0.82
397	Bupivacaine	Ion channels	1.01
398	Ondansetron	Ion channels	0.75
399	Propafenone	Ion channels	0.77
400	ATP	Ion channels	0.8
401	Phenytoin	Ion channels	1.05
402	Lacidipine	Ion channels	1.04
403	Ibutilide	Ion channels	0.7
404	Zonisamide	Ion channels	0.69
405	Pancuronium	Ion channels	0.77
406	Varenicline	Ion channels	1.45
407	Cisatracurium	Ion channels	0.78

408	Etomidate	Ion channels	0.94
409	Mexiletine	Ion channels	1.03
410	Gabapentin	Ion channels	0.86
411	Benidipine	Ion channels	1
412	Lomerizine	Ion channels	0.93
413	Amiloride	Ion channels	0.68
414	Nisoldipine	Ion channels	0.88
415	Amlodipine	Ion channels	0.76
416	Nimodipine	Ion channels	0.96
417	Nicotinic	Ion channels	0.88
418	Lamotrigine	Ion channels	1.04
419	Pramoxine	Ion channels	0.92
420	Divalproex	Ion channels	1.04
421	Felodipine	Ion channels	1.15
422	Felbamate	Ion channels	0.96
423	Benzocaine	Ion channels	1.14
424	Ropivacaine	Ion channels	0.99
425	Manidipine	Ion channels	1.07
426	Carbamazepine	Ion channels	1.02
427	Palonosetron	Ion channels	0.99
428	Azelnidipine	Ion channels	0.72
429	Flumazenil	Ion channels	1.02
430	Vitamin D3	Nuclear receptors	1.03
431	Dichlorisone	Nuclear receptors	0.73
432	Toremifene	Nuclear receptors	0.82
433	Fluorometholone	Nuclear receptors	0.65
434	Ethisterone	Nuclear receptors	1.13
435	Fluocinonide	Nuclear receptors	0.98
436	Adapalene	Nuclear receptors	0.87
437	Flutamide	Nuclear receptors	0.97
438	Hydrocortisone	Nuclear receptors	0.91
439	Medrysone	Nuclear receptors	0.73
440	Betamethasone	Nuclear receptors	1.07
441	Ursodiol	Nuclear receptors	0.63
442	Desonide	Nuclear receptors	0.97
443	Loteprednol	Nuclear receptors	0.91
444	Rosiglitazone	Nuclear receptors	0.95
445	Ethynodiol	Nuclear receptors	0.95
446	Pioglitazone	Nuclear receptors	0.86
447	Estradiol valerate	Nuclear receptors	1.09
448	Mifepristone	Nuclear receptors	1.1
449	Spironolactone	Nuclear receptors	1.03
450	Fenofibrate	Nuclear receptors	0.83
451	Betamethasone	Nuclear receptors	0.93
452	Megestrol	Nuclear receptors	0.88
453	Meprednisone	Nuclear receptors	0.93
454	Canrenoate	Nuclear receptors	1.08
455	Liothyronine	Nuclear receptors	0.96
456	Tiratricol	Nuclear receptors	0.8
457	Estrone	Nuclear receptors	0.89
458	Fluticasone	Nuclear receptors	1.76

459	Budesonide	Nuclear receptors	0.92
460	Fulvestrant	Nuclear receptors	0.97
461	Tamoxifen	Nuclear receptors	0.88
462	Bexarotene	Nuclear receptors	1.08
463	Dexamethasone	Nuclear receptors	0.86
464	Oxymetholone	Nuclear receptors	0.98
465	Tazarotene	Nuclear receptors	1.19
466	Flumethasone	Nuclear receptors	1.04
467	Bazedoxifene	Nuclear receptors	0.95
468	Halobetasol Propionate	Nuclear receptors	1.09
469	Diethylstilbestrol	Nuclear receptors	0.82
470	Mestranol	Nuclear receptors	0.85
471	Dydrogesterone	Nuclear receptors	0.79
472	Estradiol	Nuclear receptors	0.85
473	Rosiglitazone	Nuclear receptors	0.91
474	butyrate	Nuclear receptors	0.71
475	Difluprednate	Nuclear receptors	1.02
476	Mometasone	Nuclear receptors	0.73
477	Triamcinolone	Nuclear receptors	0.89
478	Deflazacort	Nuclear receptors	0.7
479	Fluocinolone	Nuclear receptors	0.96
480	Tretinoin	Nuclear receptors	0.95
481	Calcitriol	Nuclear receptors	1.39
482	Dexamethasone	Nuclear receptors	1.01
483	Doxercalciferol	Nuclear receptors	1.45
484	Estriol	Nuclear receptors	0.75
485	Altrenogest	Nuclear receptors	0.8
486	Betamethasone	Nuclear receptors	0.9
487	Calcifediol	Nuclear receptors	1.17
488	Alfacalcidol	Nuclear receptors	0.87
489	Clofibrate	Nuclear receptors	0.87
490	Triamcinolone	Nuclear receptors	0.9
491	Nateglinide	Transporters	1.03
492	Reboxetine	Transporters	0.81
493	Imipramine	Transporters	1.06
494	Gliclazide	Transporters	0.91
495	Bendroflumethiazide	Transporters	0.86
496	Amitriptyline	Transporters	1.04
497	Benzthiazide	Transporters	1.06
498	Ivacaftor	Transporters	ND
499	Methyclothiazide	Transporters	0.94
500	Indapamide	Transporters	0.84
501	Venlafaxine	Transporters	1.04
502	Sertraline	Transporters	1.06
503	Tolbutamide	Transporters	1.01
504	Mitiglinide	Transporters	0.91
505	Repaglinide	Transporters	1.02
506	Dapoxetine	Transporters	0.83
507	Gliquidone	Transporters	1.26
508	Duloxetine	Transporters	0.74
509	Torsemide	Transporters	0.96

510	Chlorothiazide	Transporters	0.96
511	Paroxetine	Transporters	0.55
512	Trimipramine	Transporters	0.44
513	Fluvoxamine	Transporters	0.96
514	Trichlormethiazide	Transporters	0.9
515	Glipizide	Transporters	0.88
516	Benzbromarone	Transporters	1
517	Clomipramine	Transporters	0.9
518	Tolazamide	Transporters	0.96
519	Bumetanide	Transporters	0.92
520	Amoxapine	Transporters	0.86
521	Ezetimibe	Transporters	1.17
522	Guanethidine	Transporters	0.84
523	Nicorandil	Transporters	1.09
524	Nomifensine	Transporters	0.89
525	Maprotiline	Transporters	0.78
526	Meticrane	Transporters	0.8
527	Atomoxetine	Transporters	0.89
528	Milnacipran	Transporters	1.01
529	Pinacidil	Transporters	0.94
530	Chlorpropamide	Transporters	1.07
531	Fluoxetine	Transporters	0.93
532	Everolimus	Non receptor kinases	1.07
533	Sorafenib	Non receptor kinases	1.48
534	Vemurafenib	Non receptor kinases	1
535	Phenformin	Non receptor kinases	0.94
536	Ponatinib	Non receptor kinases	1.78
537	Ibrutinib	Non receptor kinases	2.17
538	Regorafenib	Non receptor kinases	1.68
539	Metformin	Non receptor kinases	0.75
540	Dabrafenib	Non receptor kinases	0.77
541	Temsirolimus	Non receptor kinases	0.7
542	Thalidomide	Cytokines	0.98
543	Pomalidomide	Cytokines	1.12
544	Lenalidomide	Cytokines	0.76
545	Bindarit	Cytokines	1
546	Sulfanilamide	Others	0.86
547	Edaravone	Others	0.88
548	Methoxyestradiol	Others	0.94
549	Cyclamic	Others	1.07
550	Lithocholic	Others	0.87
551	Emtricitabine	Others	1.26
552	Genistein	Others	0.97
553	Valnemulin	Others	1.08
554	Monofluorophosphate	Others	0.82
555	Ethambutol	Others	1
556	Leucovorin	Others	0.79
557	Gatifloxacin	Others	1.07
558	Temozolomide	Others	0.96
559	Sulfasalazine	Others	1.29
560	Ouabain	Others	0.64

561	Clofibric	Others	0.91
562	Nitazoxanide	Others	1
563	Azaperone	Others	0.61
564	Nithiamide	Others	0.65
565	Allylthiourea	Others	0.86
566	Cysteamine	Others	0.85
567	Zoxazolamine	Others	0.93
568	Phenazopyridine	Others	0.72
569	Penciclovir	Others	0.95
570	Vincristine	Others	0.94
571	Clinafloxacin	Others	0.67
572	Natamycin	Others	0.93
573	Ritonavir	Others	1.04
574	Alverine Citrate	Others	0.72
575	Didanosine	Others	1.04
576	Besifloxacin	Others	0.98
577	Amidopyrine	Others	1.28
578	Triclabendazole	Others	0.61
579	Dicloxacillin	Others	0.98
580	Vinorelbine	Others	1.15
581	Chlorocresol	Others	1.13
582	Telaprevir	Others	0.99
583	Isovaleramide	Others	1.04
584	Danofloxacin	Others	0.68
585	Sulconazole	Others	0.7
586	Enrofloxacin	Others	0.68
587	Tilmicosin	Others	0.92
588	Ethionamide	Others	0.95
589	Thiamine	Others	0.91
590	Troxipide	Others	0.96
591	Fluconazole	Others	1.03
592	Ellagic	Others	1.08
593	Fidaxomicin	Others	0.97
594	Clodronate	Others	1.04
595	Minocycline	Others	0.9
596	Diminazene	Others	1.19
597	Cinepazide	Others	1.11
598	Sucralose	Others	0.99
599	Praziquantel	Others	1.01
600	Mevastatin	Others	0.64
601	Suprofen	Others	1.01
602	Doxycycline	Others	0.77
603	Dirithromycin	Others	1.03
604	Pemirolast	Others	0.63
605	Ranolazine	Others	0.91
606	Busulfan	Others	0.97
607	Cisplatin	Others	0.83
608	Dibenzepine	Others	0.78
609	Cepharanthine	Others	0.83
610	Phenacetin	Others	0.87
611	Spectinomycin	Others	0.94

612	Thonzonium	Others	1.05
613	Thiostrepton	Others	0.97
614	Camptothecin	Others	1.07
615	Rolitetracycline	Others	0.96
616	Rapamycin	Others	0.94
617	Oxeladin	Others	0.99
618	Carbadox	Others	1.04
619	Piromidic	Others	1.06
620	Deoxyarbutin	Others	0.9
621	Monobenzone	Others	0.78
622	Clindamycin	Others	0.99
623	Pantothenic acid	Others	0.95
624	Cephalomannine	Others	0.95
625	Sarafloxacin	Others	0.95
626	Pentoxifylline	Others	0.95
627	Moxalactam	Others	1.05
628	Camylofin	Others	0.9
629	Benfotiamine	Others	0.65
630	Methapyrilene	Others	0.43
631	Clofazimine	Others	1.1
632	Pentamidine	Others	1.13
633	Cefaclor	Others	0.84
634	Amoxicillin	Others	1.05
635	Artemisinin	Others	0.92
636	Telbivudine	Others	0.93
637	Aniracetam	Others	0.79
638	Catharanthine	Others	0.99
639	Tranilast	Others	1.76
640	Buflomedil	Others	1.14
641	Lomefloxacin	Others	1.01
642	Moroxydine	Others	0.88
643	Ginkgolide	Others	1.05
644	Metrizamide	Others	1.06
645	Methylhydantoin	Others	1.1
646	Voriconazole	Others	0.99
647	Pridinol Methanesulfonate	Others	1.01
648	Tioconazole	Others	0.96
649	Penicillin	Others	0.91
650	Flumequine	Others	1.08
651	Atazanavir	Others	0.83
652	Ofloxacin	Others	0.85
653	Fenbendazole	Others	1.14
654	Dextrose	Others	0.92
655	Marbofloxacin	Others	0.82
656	Pyrimethamine	Others	0.93
657	Suxibuzone	Others	0.87
658	Phthalylsulfacetamide	Others	0.92
659	Phenothrin	Others	0.91
660	Noscapine	Others	0.94
661	Glafenine	Others	1.5
662	Cinoxacin	Others	0.86

663	aminohippurate Hydrate	Others	0.87
664	Primaquine	Others	0.91
665	Mepiroxol	Others	0.94
666	Hemicholinium	Others	0.86
667	Clofoctol	Others	1.09
668	Cephapirin	Others	0.89
669	Gluceptate	Others	0.89
670	Butacaine	Others	0.71
671	Auranofin	Others	2.62
672	Aztreonam	Others	0.85
673	Aminoacridine	Others	0.93
674	Docetaxel	Others	0.66
675	Alexidine	Others	ND
676	Ethacridine	Others	0.99
677	Potassium Iodide	Others	0.86
678	Digoxigenin	Others	0.89
679	Guanidine	Others	0.88
680	Bentiromide	Others	0.85
681	Fosfomycin	Others	0.64
682	Difloxacin	Others	0.89
683	Bekanamycin	Others	0.83
684	Paclitaxel	Others	0.85
685	Proadifen	Others	0.81
686	ascorbate	Others	0.99
687	Deoxycorticosterone	Others	0.81
688	Cetrimonium Bromide	Others	1.89
689	Norfloxacin	Others	0.97
690	Bergapten	Others	0.98
691	Bephenium	Others	0.79
692	Diperodon	Others	0.77
693	Isoxicam	Others	0.72
694	Malotilate	Others	0.87
695	Famprofazone	Others	0.82
696	Piperacillin	Others	0.98
697	Ifosfamide	Others	0.77
698	Spiramycin	Others	0.75
699	Phosphatidylcholine	Others	0.51
700	Procodazole	Others	0.94
701	Amorolfine	Others	0.85
702	Chloramphenicol	Others	0.83
703	Picrotoxinin	Others	0.72
704	Pasiniazid	Others	0.96
705	Sulbactam	Others	0.48
706	Emetine	Others	0.67
707	Streptozotocin	Others	0.66
708	Mesalamine	Others	0.76
709	Dimaprit	Others	0.81
710	Dibenzothiophene	Others	0.95
711	Colistimethate	Others	0.79
712	Clorgyline	Others	0.86
713	Clopamide	Others	0.56

714	Hydrastinine	Others	0.99
715	Clinafoxacin	Others	0.95
716	Chromocarb	Others	0.93
717	Ceftazidime	Others	0.83
718	Nifenazone	Others	1.02
719	Cephalexin	Others	0.93
720	Meclocycline	Others	0.65
721	Isosorbide	Others	0.86
722	Azaguanine	Others	1.12
723	Furaltadone	Others	0.82
724	Ceftiofur	Others	1.03
725	Resveratrol	Others	0.72
726	Clindamycin	Others	0.71
727	Levofloxacin	Others	0.75
728	Riboflavin	Others	ND
729	Dyclonine	Others	0.92
730	Sorbitol	Others	0.92
731	carnitine	Others	1.07
732	Mannitol	Others	0.72
733	Metronidazole	Others	0.92
734	Menadione	Others	0.82
735	Nalidixic acid	Others	0.97
736	Cefprozil	Others	0.93
737	Avobenzone	Others	1.03
738	Artemether	Others	1.15
739	Talc	Others	0.97
740	Methoxsalen	Others	0.76
741	Nicotinamide	Others	0.88
742	Miconazole	Others	0.73
743	Acetanilide	Others	0.79
744	Sulfamethizole	Others	0.87
745	Secnidazole	Others	0.84
746	Famciclovir	Others	0.95
747	Miconazole	Others	0.65
748	Econazole nitrate	Others	0.73
749	Adiphenine	Others	0.86
750	Carnitine	Others	0.78
751	Isoconazole	Others	0.75
752	Scopine	Others	1
753	Isoniazid	Others	0.69
754	Clindamycin	Others	1.06
755	Bisacodyl	Others	0.97
756	Pramiracetam	Others	1.03
757	Clarithromycin	Others	1.09
758	Vidarabine	Others	0.78
759	Aminolevulinic	Others	1.48
760	Azacyclonol	Others	0.81
761	Irsogladine	Others	1.23
762	Amfebutamone	Others	1.18
763	Alibendol	Others	1.12
764	Mecarbinate	Others	1.14

765	Moxifloxacin	Others	0.98
766	Clindamycin	Others	0.83
767	Rifaximin	Others	0.98
768	Geniposidic	Others	0.93
769	Sulfisoxazole	Others	1.15
770	Genipin	Others	1.07
771	Sulfamethoxazole	Others	0.99
772	Geniposide	Others	1
773	Pregnenolone	Others	0.99
774	Paeoniflorin	Others	0.9
775	Deacetylbaccatin	Others	0.85
776	Cromoglycate	Others	0.94
777	Sulbactam	Others	0.81
778	Oxytetracycline	Others	1.07
779	Nystatin	Others	0.88
780	Crystal Violet	Others	ND
781	Rebamipide	Others	0.77
782	Acadesine	Others	0.82
783	Fenticonazole	Others	0.63
784	Azithromycin	Others	1.72
785	Albendazole	Others	0.99
786	Flunixin	Others	0.99
787	Etidronate	Others	0.73
788	Xylose	Others	0.71
789	Raltegravir	Others	0.79
790	Elvitegravir	Others	0.87
791	Roxithromycin	Others	0.8
792	orthovanadate	Others	0.91
793	Ribavirin	Others	0.78
794	Cycloserine	Others	0.68
795	Liranaftate	Others	0.68
796	Fudosteine	Others	0.7
797	Quinine	Others	0.66
798	Procarbazine	Others	0.79
799	Licofelone	Others	0.78
800	Bifonazole	Others	0.61
801	Arbidol	Others	1.07
802	Penicillamine	Others	0.83
803	Probucol	Others	0.71
804	Oxibendazole	Others	0.9
805	Daidzein	Others	0.71
806	Curcumin	Others	1.76
807	Chloroxine	Others	1.16
808	Vinpocetine	Others	0.67
809	Lomustine	Others	0.69
810	Novobiocin	Others	1.1
811	Butoconazole	Others	0.7
812	Valaciclovir	Others	0.5
813	Oxfendazole	Others	1.25
814	Ciclopirox	Others	0.81
815	Methacycline	Others	0.8

816	Lopinavir	Others	1.06
817	Acipimox	Others	0.92
818	Ciprofloxacin	Others	0.84
819	Aciclovir	Others	0.81
820	DAPT	Others	0.73
821	Fleroxacin	Others	0.87
822	Sulphadimethoxine	Others	0.83
823	Rimantadine	Others	1.2
824	Sparfloxacin	Others	1.01
825	Primidone	Others	0.87
826	Idoxuridine	Others	1.1
827	Pivoxil	Others	0.96
828	Protionamide	Others	0.71
829	Itraconazole	Others	1.21
830	Nefiracetam	Others	0.92
831	Lincomycin	Others	0.85
832	Chlormezanone	Others	1
833	Cidofovir	Others	0.89
834	Erdosteine	Others	0.96
835	Suplatast	Others	0.84
836	Tobramycin	Others	0.79
837	Taurine	Others	1.29
838	Sulfadoxine	Others	1.16
839	Sitafloxacin	Others	0.77
840	Ganciclovir	Others	0.83
841	Trifluridine	Others	0.68
842	Oseltamivir	Others	1.02
843	Verteporfin	Others	ND
844	Valganciclovir	Others	0.88
845	Cyclandelate	Others	1.01
846	Antipyrine	Others	0.84
847	Sasapyrine	Others	0.96
848	Enoxacin	Others	0.89
849	Salicylanilide	Others	0.87
850	Ampicillin	Others	0.91
851	Domiphen	Others	1.22
852	Abacavir	Others	0.68
853	Sulfacetamide	Others	0.9
854	Amoxicillin	Others	0.91
855	Linezolid	Others	0.93
856	Rifapentine	Others	1.2
857	L-Arginine	Others	1.02
858	Amprenavir	Others	0.99
859	Zanamivir	Others	0.59
860	Mequinol	Others	0.64
861	Albendazole	Others	1.12
862	L-Thyroxine	Others	1.11
863	Carbazochrome	Others	0.93
864	Flucytosine	Others	0.62
865	Hygromycin	Others	0.71
866	Aminosalicylate	Others	0.7

867	Decamethonium	Others	0.87
868	Paromomycin Sulfate	Others	0.88
869	Tylosin tartrate	Others	0.98
870	Nifuroxazide	Others	0.85
871	Posaconazole	Others	1.21
872	Sertaconazole	Others	0.62
873	Cinchophen	Others	0.96
874	Chlorquinaldol	Others	0.97
875	Azlocillin	Others	0.88
876	Florfenicol	Others	0.73
877	Tolperisone	Others	0.85
878	Octopamine	Others	0.72
879	Vinblastine	Others	1.13
880	Aminothiazole	Others	0.91
881	Bemegride	Others	1.05
882	Carboplatin	Others	0.98
883	Erythromycin	Others	1.04
884	Amphotericin	Others	0.96
885	Niclosamide	Others	0.91
886	Fenspiride	Others	1.04
887	Betamipron	Others	1
888	PMSF	Others	1
889	Teicoplanin	Others	0.88
890	Cabazitaxel	Others	1
891	Tenofovir	Others	0.83
892	Tenofovir	Others	1.02
893	Glutamine	Others	0.85
894	Ciclopirox	Others	0.78
895	Tigecycline	Others	0.88
896	Gadodiamide	Others	0.95
897	Broxyquinoline	Others	1.44
898	Carbenicillin	Others	0.98
899	Chenodeoxycholic	Others	0.74
900	Entecavir Hydrate	Others	0.86
901	Stavudine	Others	0.98
902	Nefopam	Others	0.86
903	Hexadecanol	Others	0.97
904	Naftifine	Others	1
905	Sulfadiazine	Others	0.76
906	Dehydroepiandrosterone	Others	1.04
907	Idebenone	Others	1.2
908	Erythromycin	Others	1.06
909	Retapamulin	Others	1
910	Trimethoprim	Others	1.01
911	Oxytetracycline	Others	0.99
912	Ranolazine	Others	0.81
913	Cytarabine	Others	1.14
914	Ronidazole	Others	1.13
915	Cetylpyridinium	Others	1.41
916	Carotene	Others	0.87
917	Coumarin	Others	0.97

918	Biotin	Others	1
919	Pefloxacin Mesylate	Others	0.96
920	Methenamine	Others	1.03
921	Cyromazine	Others	0.96
922	Benzethonium	Others	1.82
923	Cefditoren	Others	0.84
924	Sulfamerazine	Others	1.02
925	Rifampin	Others	0.84
926	Clorsulon	Others	1.1
927	Sulfamethazine	Others	0.96
928	Nitrofural	Others	0.69
929	Sulfaguanidine	Others	1.08
930	Trometamol	Others	1
931	Tianeptine	Others	0.82
932	Deferiprone	Others	0.8
933	Netilmicin	Others	0.99
934	Pyrazinamide	Others	0.93
935	Tinidazole	Others	0.8
936	Peramivir	Others	1.23
937	Climbazole	Others	0.92
938	Dequalinium	Others	1.29
939	Tioxolone	Others	1.08
940	Mezlocillin	Others	0.95
941	Arecoline	Others	1
942	Butenafine	Others	1.16

Comounds in the plate unsatisfied Z'-factor

#	**Name**	**Target**
1	Silodosin	Membrane receptors
2	Pizotifen	Membrane receptors
3	Fumarate	Membrane receptors
4	Clorprenaline	Membrane receptors
5	Naloxone	Membrane receptors
6	Brompheniramine	Membrane receptors
7	Mianserin	Membrane receptors
8	Telmisartan	Membrane receptors
9	Mosapride	Membrane receptors
10	Risperidone	Membrane receptors
11	Methylsulfate	Membrane receptors
12	Trazodone	Membrane receptors
13	Homatropine	Membrane receptors
14	Melatonin	Membrane receptors
15	Bisoprolol fumarate	Membrane receptors
16	Olmesartan	Membrane receptors
17	Imiquimod	Membrane receptors
18	Hydroxyzine	Membrane receptors
19	Indacaterol	Membrane receptors
20	Dexmedetomidine	Membrane receptors

21	Rizatriptan	Membrane receptors
22	Phenylephrine	Membrane receptors
23	Candesartan	Membrane receptors
24	Oxybutynin	Membrane receptors
25	Isoprenaline	Membrane receptors
26	Lafutidine	Membrane receptors
27	Aclidinium	Membrane receptors
28	baclofen	Membrane receptors
29	Paliperidone	Membrane receptors
30	Tetrahydrozoline	Membrane receptors
31	Levodopa	Membrane receptors
32	Roxatidine	Membrane receptors
33	Terazosin	Membrane receptors
34	Xylometazoline	Membrane receptors
35	Loratadine	Membrane receptors
36	Fludarabine	Enzymes
37	Doxorubicin	Enzymes
38	Indomethacin	Enzymes
39	Fluorouracil	Enzymes
40	Methotrexate	Enzymes
41	Clofarabine	Enzymes
42	Methazolamide	Enzymes
43	Idarubicin	Enzymes
44	Apixaban	Enzymes
45	Quinapril	Enzymes
46	Pyridostigmine	Enzymes
47	Lovastatin	Enzymes
48	Tolcapone	Enzymes
49	Decitabine	Enzymes
50	Epirubicin	Enzymes
51	Hydralazine	Enzymes
52	Dexrazoxane	Enzymes
53	Etoposide	Enzymes
54	Ubenimex	Enzymes
55	Flavoxate	Enzymes
56	Dorzolamide	Enzymes
57	Mitotane	Enzymes
58	Dutasteride	Enzymes
59	Gemcitabine	Enzymes
60	Fenoprofen	Enzymes
61	Piroxicam	Enzymes
62	Miglitol	Enzymes
63	Omeprazole	Enzymes
64	Carprofen	Enzymes
65	Mizoribine	Enzymes
66	Ketoconazole	Enzymes
67	Lansoprazole	Enzymes
68	Meloxicam	Enzymes
69	Riluzole	Ion channels
70	Granisetron	Ion channels
71	Penfluridol	Ion channels

72	Oxcarbazepine	Ion channels
73	Procaine	Ion channels
74	Prilocaine	Ion channels
75	Dibucaine	Ion channels
76	Lidocaine	Ion channels
77	Tetracaine	Ion channels
78	Amiloride	Ion channels
79	Ondansetron	Ion channels
80	Rosiglitazone	Nuclear receptors
81	Beclomethasone	Nuclear receptors
82	Medroxyprogesterone	Nuclear receptors
83	Prednisolone	Nuclear receptors
84	Clomifene	Nuclear receptors
85	Cortisone	Nuclear receptors
86	Prednisolone	Nuclear receptors
87	Ulipristal	Nuclear receptors
88	Bezafibrate	Nuclear receptors
89	Norethindrone	Nuclear receptors
90	Vitamin C	Nuclear receptors
91	Pioglitazone	Nuclear receptors
92	Gestodene	Nuclear receptors
93	Drospirenone	Nuclear receptors
94	Isotretinoin	Nuclear receptors
95	Gemfibrozil	Nuclear receptors
96	Estradiol	Nuclear receptors
97	Levonorgestrel	Nuclear receptors
98	Eplerenone	Nuclear receptors
99	Methylprednisolone	Nuclear receptors
100	Clobetasol	Nuclear receptors
101	Progesterone	Nuclear receptors
102	Prednisone	Nuclear receptors
103	Acitretin	Nuclear receptors
104	Raloxifene	Nuclear receptors
105	Levetiracetam	Transporters
106	Hydrochlorothiazide	Transporters
107	Minoxidil	Transporters
108	Furosemide	Transporters
109	Glyburide	Transporters
110	Metolazone	Transporters
111	Reserpine	Transporters
112	Glimepiride	Transporters
113	Pidotimod	Others
114	Ornidazole	Others
115	Chloroquine	Others
116	Sulfathiazole	Others
117	Chlorzoxazone	Others
118	Caspofungin	Others
119	Dropropizine	Others
120	Flubendazole	Others
121	Pyridoxine	Others
122	D-Phenylalanine	Others

123	Eprazinone	Others
124	Chlortetracycline	Others
125	Thiamphenicol	Others
126	Ethamsylate	Others
127	Vitamin D2	Others
128	Olsalazine	Others
129	levofolinate	Others
130	Zidovudine	Others
131	Nafcillin	Others
132	Ampicillin	Others
133	Azithromycin	Others
134	Amprolium	Others
135	Toltrazuril	Others
136	Bacitracin	Others
137	Acetylcysteine	Others
138	Orbifloxacin	Others
139	Doxapram	Others
140	Moguisteine	Others
141	Atovaquone	Others
142	Nadifloxacin	Others
143	Creatinine	Others
144	Decoquinate	Others
145	Rifabutin	Others
146	Nevirapine	Others
147	Sulfapyridine	Others
148	Amikacin	Others
149	Cefoperazone	Others
150	Clafen	Others
151	Altretamine	Others
152	Terbinafine	Others
153	Doripenem	Others
154	Azathioprine	Others
155	Daptomycin	Others
156	Zalcitabine	Others
157	Cefoselis	Others
158	Adefovir	Others
159	Biapenem	Others
160	Bleomycin	Others
161	Nelarabine	Others
162	Clotrimazole	Others
163	Bendamustine	Others
164	Cefdinir	Others
165	Deferasirox	Others
166	Ivermectin	Others
167	Lamivudine	Others
168	Sulfameter	Others
169	Darunavir	Others
170	Dacarbazine	Others
171	Oxacillin	Others
172	Streptomycin	Others
173	Probenecid	Others

174	Neomycin	Others
175	Picosulfate	Others
176	Cloxacillin	Others
177	Colistin	Others
178	Meropenem	Others
179	Balofloxacin	Others
180	Tiopronin	Others
181	Bromhexine	Others
182	Tolnaftate	Others
183	Cyclophosphamide	Others
184	Docosanol	Others
185	Guaifenesin	Others
186	Thiabendazole	Others
187	Vancomycin	Others
188	Nafamostat	Others
189	Methocarbamol	Others
190	Mesna	Others
191	Terbinafine	Others
192	Tetracycline	Others

References

[1] L. Tiefenauer and S. Demarche, “Challenges in the development of functional assays of membrane proteins,” 2012. doi: 10.3390/ma5112205.

[2] R. Santos et al., “A comprehensive map of molecular drug targets,” Nat Rev Drug Discov, vol. 16, no. 1, pp. 19–34, Dec. 2016, doi: 10.1038/nrd.2016.230.

[3] A. L. Hopkins and C. R. Groom, “The druggable genome,” Nat Rev Drug Discov, vol. 1, no. 9, pp. 727–730, 2002, doi: 10.1038/nrd892.

[4] “Complementary Approaches to Existing Target Based Drug Discovery for Identifying Novel Drug Targets - biomedicines-04-00027”.

[5] “Epidermal growth factor receptor tyrosine kinase inhibitors (EGFR-TKIs)_ Simple drugs with a complex mechanism of action_ - Journal Cellular Physiology - 2002 - Normanno - Epidermal growth factor receptor tyrosine kinase inhibitors EGFR-TKIs ”.

[6] M. Roengvoraphoj, G. J. Tsongalis, K. H. Dragnev, and J. R. Rigas, “Epidermal growth factor receptor tyrosine kinase inhibitors as initial therapy for non-small cell lung cancer: Focus on epidermal growth factor receptor mutation testing and mutation-positive patients,” Cancer Treat Rev, vol. 39, no. 8, pp. 839–850, Dec. 2013, doi: 10.1016/J.CTRV.2013.05.001.

[7] M. Chiba et al., “Efficacy of irreversible EGFR-TKIs for the uncommon secondary resistant EGFR mutations L747S, D761Y, and T854A,” BMC Cancer, vol. 17, no. 1, Apr. 2017, doi: 10.1186/s12885-017-3263-z.

[8] Y. R. Chen et al., “Distinctive activation patterns in constitutively active and gefitinib-sensitive EGFR mutants,” Oncogene, vol. 25, no. 8, pp. 1205–1215,

Feb. 2006, doi: 10.1038/sj.onc.1209159.

[9] Du X et al., “Acquired resistance to third-generation EGFR-TKIs and emerging next-generation EGFR inhibitors,” Innovation (Camb), vol. 3;2(2), p. 100, Apr. 2021.

[10] I. Galdadas, L. Carlino, R. A. Ward, S. J. Hughes, S. Haider, and F. L. Gervasio, “Structural basis of the effect of activating mutations on the EGF receptor,” Elife, vol. 10, Jul. 2021, doi: 10.7554/eLife.65824.

[11] M. Tokumo et al., “The Relationship between Epidermal Growth Factor Receptor Mutations and Clinicopathologic Features in Non-Small Cell Lung Cancers.” [Online]. Available: http://aacrjournals.org/clincancerres/article-pdf/11/3/1167/1963588/1167-1173.pdf

[12] R. I. Nicholson, J. M. W. Gee, and M. E. Harper, “EGFR and cancer prognosis,” Eur J Cancer, vol. 37, no. SUPPL. 4, pp. 9–15, Sep. 2001, doi: 10.1016/S0959-8049(01)00231-3.

[13] J. Gao, J. Jian, Z. Jiang, and A. Van Schepdael, “Screening assays for tyrosine kinase inhibitors: A review,” J Pharm Biomed Anal, vol. 223, p. 115166, Jan. 2023, doi: 10.1016/J.JPBA.2022.115166.

[14] P. Wee and Z. Wang, “Epidermal growth factor receptor cell proliferation signaling pathways,” May 17, 2017, MDPI AG. doi: 10.3390/cancers9050052.

[15] Y. Sako, S. Minoguchi, and T. Yanagida, “Single-molecule imaging of EGFR signalling on the surface of living cells,” 2000.

[16] “Single-Molecule Analysis of Chemotactic Signaling in Dictyostelium Cells - science.1063951”.

[17] R. Iino, I. Koyama, and A. Kusumi, “Single Molecule Imaging of Green

Fluorescent Proteins in Living Cells: E-Cadherin Forms Oligomers on the Free Cell Surface," Biophys J, vol. 80, no. 6, pp. 2667–2677, Jun. 2001, doi: 10.1016/S0006-3495(01)76236-4.

[18] M. Hiroshima, C. gi Pack, K. Kaizu, K. Takahashi, M. Ueda, and Y. Sako, "Transient Acceleration of Epidermal Growth Factor Receptor Dynamics Produces Higher-Order Signaling Clusters," J Mol Biol, vol. 430, no. 9, pp. 1386–1401, Apr. 2018, doi: 10.1016/J.JMB.2018.02.018.

[19] H. K. Byeon, M. Ku, and J. Yang, "Beyond EGFR inhibition: multilateral combat strategies to stop the progression of head and neck cancer," Jan. 01, 2019, Nature Publishing Group. doi: 10.1038/s12276-018-0202-2.

[20] "Mu-opioid receptor and receptor tyrosine kinase crosstalk_ Implications in mechanisms of opioid tolerance, reduced analgesia to neuropathic pain, dependence, and reward - fnsys-16-1059089".

[21] D. T. Clarke and M. L. Martin-Fernandez, "A brief history of single-particle tracking of the epidermal growth factor receptor," 2019, MDPI AG. doi: 10.3390/mps2010012.

[22] M. Hiroshima, Y. Saeki, M. Okada-Hatakeyama, and Y. Sako, "Dynamically varying interactions between heregulin and ErbB proteins detected by single-molecule analysis in living cells," vol. 109, 2012, doi: 10.1073/pnas.1200464109/-/DCSupplemental.

[23] M. Hiroshima et al., "Membrane cholesterol interferes with tyrosine phosphorylation but facilitates the clustering and signal transduction of EGFR," Aug. 28, 2021. doi: 10.1101/2021.08.28.457965.

[24] M. G. Sugiyama et al., "Confinement of unliganded EGFR by tetraspanin

nanodomains gates EGFR ligand binding and signaling," Nat Commun, vol. 14, no. 1, Dec. 2023, doi: 10.1038/s41467-023-38390-z.

[25] M. Yasui, M. Hiroshima, J. Kozuka, Y. Sako, and M. Ueda, "Automated single-molecule imaging in living cells," Nat Commun, vol. 9, no. 1, Dec. 2018, doi: 10.1038/s41467-018-05524-7.

[26] C. Stringer, T. Wang, M. Michaelos, and M. Pachitariu, "Cellpose: a generalist algorithm for cellular segmentation," Nat Methods, vol. 18, no. 1, pp. 100–106, Jan. 2021, doi: 10.1038/s41592-020-01018-x.

[27] M. Pachitariu and C. Stringer, "Cellpose 2.0: how to train your own model," Nat Methods, vol. 19, no. 12, pp. 1634–1641, Dec. 2022, doi: 10.1038/s41592-022-01663-4.

[28] C. Stringer and M. Pachitariu, "Cellpose3: one-click image restoration for improved cellular segmentation," Feb. 12, 2024. doi: 10.1101/2024.02.10.579780.

[29] Y. Naruo et al., "Epidermal growth factor receptor mutation in combination with expression of MIG6 alters gefitinib sensitivity," BMC Syst Biol, vol. 5, Feb. 2011, doi: 10.1186/1752-0509-5-29.

[30] M. de Wit et al., "Mutation and drug-specific intracellular accumulation of EGFR predict clinical responses to tyrosine kinase inhibitors," EBioMedicine, vol. 56, p. 102796, Jun. 2020, doi: 10.1016/J.EBIOM.2020.102796.

[31] "zhang-et-al-1999-a-simple-statistical-parameter-for-use-in-evaluation-and-validation-of-high-throughput-screening-assays".

[32] "Globally Approved EGFR Inhibitors_ Insights into Their Syntheses, Target Kinases, Biological Activities, Receptor Interactions, and Metabolism -

molecules-26-06677".

[33] V. De Falco et al., "Ponatinib (AP24534) is a novel potent inhibitor of oncogenic RET mutants associated with thyroid cancer," Journal of Clinical Endocrinology and Metabolism, vol. 98, no. 5, May 2013, doi: 10.1210/jc.2012-2672.

[34] T. O'Hare et al., "AP24534, a Pan-BCR-ABL Inhibitor for Chronic Myeloid Leukemia, Potently Inhibits the T315I Mutant and Overcomes Mutation-Based Resistance," Cancer Cell, vol. 16, no. 5, pp. 401–412, Nov. 2009, doi: 10.1016/j.ccr.2009.09.028.

[35] R. E. Joseph, N. Amatya, D. B. Fulton, J. R. Engen, T. E. Wales, and A. H. Andreotti, "Differential impact of BTK active site inhibitors on the conformational state of full-length BTK," Elife, vol. 9, pp. 1–57, Oct. 2020, doi: 10.7554/eLife.60470.

[36] S. Yuan et al., "Screening of an FDA-approved drug library with a two-tier system identifies an entry inhibitor of severe fever with thrombocytopenia syndrome virus," Viruses, vol. 11, no. 4, Apr. 2019, doi: 10.3390/V11040385.

[37] M. Lehmann, K. D. S. P. Vilar, A. Franco, M. L. Reguly, and H. H. R. De Andrade, "Activity of topoisomerase inhibitors daunorubicin, idarubicin, and aclarubicin in the Drosophila somatic mutation and recombination test," Environ Mol Mutagen, vol. 43, no. 4, pp. 250–257, 2004, doi: 10.1002/em.20023.

[38] S. H. Lum and J. D. Grainger, "Eltrombopag for the treatment of aplastic anemia: Current perspectives," Sep. 13, 2016, Dove Medical Press Ltd. doi: 10.2147/DDDT.S95715.

[39] G. W. Carlile et al., "The NSAID glafenine rescues class 2 CFTR mutants via cyclooxygenase 2 inhibition of the arachidonic acid pathway," Sci Rep, vol. 12,

no. 1, Dec. 2022, doi: 10.1038/s41598-022-08661-8.

[40] H. M. Kantarjian et al., “Nilotinib is effective in patients with chronic myeloid leukemia in chronic phase after imatinib resistance or intolerance: 24-month follow-up results,” 2011, doi: 10.1182/blood-2010-03.

[41] C. Guevremont, C. Jeldres, and P. I. Karakiewicz, “SORAFENIB IN THE MANAGEMENT OF METASTATIC RCC U R O L O G I C O N C O L O G Y Sorafenib in the management of metastatic renal cell carcinoma,” 2009.

[42] N. Borodoker et al., “Verteporfin infusion-associated pain,” Am J Ophthalmol, vol. 133, no. 2, pp. 211–214, Feb. 2002, doi: 10.1016/S0002-9394(01)01341-1.

[43] F. A. K. L. J. G. M. L. H. N. P. A. L. and A. W. B. Walker, “Activation of the Ras/mitogen-activated protein kinase pathway by kinase-defective epidermal growth factor receptors results in cell survival but not proliferation,” Mol Cell Biol, vol. 18 (12), pp. 7192–7204, 1998.

[44] M. L. Janmaat, F. A. E. Kruyt, J. A. Rodriguez, and G. Giaccone, “Response to Epidermal Growth Factor Receptor Inhibitors in Non-Small Cell Lung Cancer Cells: Limited Antiproliferative Effects and Absence of Apoptosis Associated with Persistent Activity of Extracellular Signal-regulated Kinase or Akt Kinase Pathways.” [Online]. Available: http://aacrjournals.org/clincancerres/article-pdf/9/6/2316/2087472/df0603002316.pdf

[45] N. Giocanti, C. Hennequin, D. Rouillard, R. Defrance, and V. Favaudon, “Additive interaction of gefitinib (‘Iressa’, ZD1839) and ionising radiation in human tumour cells in vitro,” Br J Cancer, vol. 91, no. 12, pp. 2026–2033, Dec. 2004, doi: 10.1038/sj.bjc.6602242.

[46] K. Morita et al., “In Situ Synthesis of an Anticancer Peptide Amphiphile Using

Tyrosine Kinase Overexpressed in Cancer Cells," JACS Au, vol. 2, no. 9, pp. 2023–2028, Sep. 2022, doi: 10.1021/jacsau.2c00301.

[47] S. Y. Kim et al., "Effects of Clioquinol Analogues on the Hypoxia-Inducible Factor Pathway and Intracelullar Mobilization of Metal Ions," 2160.

[48] Y. Wang et al., "Hypoxia promotes ligand-independent EGF receptor signaling via hypoxia-inducible factor-mediated upregulation of caveolin-1," Proc Natl Acad Sci U S A, vol. 109, no. 13, pp. 4892–4897, Mar. 2012, doi: 10.1073/pnas.1112129109.

[49] E. Bourseau-Guilmain et al., "Hypoxia regulates global membrane protein endocytosis through caveolin-1 in cancer cells," Nat Commun, vol. 7, Apr. 2016, doi: 10.1038/ncomms11371.

[50] M. Yanagawa et al., "Single-molecule diffusion-based estimation of ligand effects on G protein-coupled receptors," 2018. [Online]. Available: www.pymol.org/

[51] K. Kawakami et al., "Heterotrimeric Gq proteins act as a switch for GRK5/6 selectivity underlying β-arrestin transducer bias," Nat Commun, vol. 13, no. 1, Dec. 2022, doi: 10.1038/s41467-022-28056-7.

[52] D. T. McSwiggen et al., "A high-throughput platform for single-molecule tracking identifies drug interaction and cellular mechanisms," May 13, 2024. doi: 10.7554/eLife.93183.2.

Publication List

Watanabe, D., Hiroshima, M., Yasui, M., & Ueda, M. (2024). Single molecule tracking based drug screening. *Nature communications*, *15*(1), 8975. https://doi.org/10.1038/s41467-024-53432-w

Takayama, M., Maeda, S., Watanabe, D., Takebayashi, K., Hiroshima, M., & Ueda, M. (2024). Cholesterol suppresses spontaneous activation of EGFR-mediated signal transduction. *Biochemical and biophysical research communications*, *704*, 149673. https://doi.org/10.1016/j.bbrc.2024.149673

国際出願番号: PCT/JP2024/007599
発明者：上田昌宏、廣島通夫、渡邉 大介
発明の名称： 受容体型チロシンキナーゼの活性評価方法
出願人：大阪大学、独立行政法人理化学研究所
出願日： 2024 年 2 月 29 日

出願番号：特願 2023-31358
発明者：上田昌宏、廣島通夫、渡邉 大介
発明の名称： 1 分子イメージングを用いた上皮成長因子受容体 EGFR の活性評価に基づく薬剤スクリーニング法
出願人：大阪大学、独立行政法人理化学研究所
出願日：2023 年 3 月 1 日

List of conference presentation

(1) Watanabe, D., Hiroshima, M. and Ueda, M. (2023) “Application of Single-molecule tracking to Drug discovery”, 2024 International Union for Pure and Applied Biophysics, 令和 6 年 6 月 24 日（月）～6 月 28 日（金）開催 国際会館, 京都 ポスター発表

(2) Watanabe, D., Hiroshima, M. and Ueda, M. (2024) “Automated Single-molecule imaging of EGFR for Drug discovery”, 2024, NTU-OsakaU Bilateral Symposium on Systems Biology in Human Disease, 令和 6 年 4 月 11 日（木）開催 国立台湾大学, 台北　口頭発表

(3) 渡邉大介、廣島通夫、上田昌宏（2024）“大規模１分子イメージング装置を用いた薬剤スクリーニング法の創出”, 第１回関西生物物理学研究会, 令和６年３月１８日（金）～３月１９日（土）開催, 大阪大学豊中キャンパス, 大阪.　ポスター発表

(4) 渡邉大介、廣島通夫、上田昌宏（2024）“細胞内１分子自動観察システムによる分子運動に基づいた薬剤スクリーニング法”, 生体運動研究合同班会議, 令和６年１月５日（金）～１月７日（日）開催、理化学研究所　神戸キャンパス（西エリア）発生・再生研究棟 C 棟１階オーディトリアム, 兵庫.　ポスター発表

(5) 渡邉大介、廣島通夫、上田昌宏（2023）“1 分子動態を指標とした薬剤スクリーニング法の開発”, 研究会「理論と実験」２０２３, 令和５年１０月５日（木）～１０月６日（金）開催、広島大学　理学部棟 E 棟２０３大会議室, 広島.　ポスター発表

(6) Daisuke Watanabe, Michio Hiroshima, Masahiro Ueda (2022) “Single molecule tracking based drug screening in living cells”, 第 60 回日本生物物理学会年会, 令和 4 年 9 月 28 日(水)～30 日(金)開催, 9 月 28 日発表。函館アリーナ・函館市民会館。函館　ポスター発表

(7) 渡邉大介、廣島通夫、上田昌宏（2019）“発がん関連遺伝子変異 EGFR の１分子動態解析”, 研究会「理論と実験」２０１９, 令和５年１０月１０日（木）～１０月１１日（金）開催、広島大学　理学部棟・学士会館, 広島.　ポスター発表

Acknowledgements

Osaka University
Prof. Masahiro Ueda
Prof. Akihiko Ishijima
Prof. Seiji Takashima
Prof. Daichi Inoue
Dr. Michio Hiroshima
Dr. Takayuki Ariga
Dr. Satomi Matsuoka
Dr. Jun Aoki
Dr Kazutoshi Takebayashi
Mr. Koji Iwamoto
Mr. Atsuhiro Mii
Mr. Cheng Guangyu
Mr. Huang Libojue
Mr. Masaki Muromoto
Mr. Keito Kimura
Mr. Yuta Sato
Ms. Haruka Yoshinari
Ms. Kaho Yamamoto
Ms. Sakura Maeda
Ms. Rena Izumi
Mr. Gai Ohashi
Mr. Yuto Akaike
Mr. Dai Sakamoto
Ms. Tomoka Higashi

RIKEN BDR
Ms. Kaori Tanabe
Ms. Shizuka Taguchi
Ms. Akiko Kanayama

Zido, Ltd.
Dr. Masato Yasui
Dr. Seiya Fukushima

I would like to thank Professor Masahiro Ueda for helping and supporting my study. And I would also like to express my appreciation to Dr. Michio Hiroshima for his technical skills and advice on data acquisition, experimental operations measurement. I am grateful for the daily assistance provided by technical staff at RIKEN BDR. I would like to express my sincere thanks to Professor Akihiko Ishijima, Professors Seiji Takashima and Daichi Inoue for reviewing this work.